The identification of novel cys-loop receptor genes in *Dirofilaria immitis*

by

Jennifer S. Nichols

A thesis submitted to the
School of Graduate and Postdoctoral Studies in partial
fulfillment of the requirements for the degree of

Masters of Science

in

Applied Bioscience

Faculty of Science

University of Ontario Institute of Technology (Ontario Tech University)

Oshawa, Ontario, Canada

October 2023

THESIS EXAMINATION INFORMATION

Submitted by: **Jennifer S. Nichols**

Master of Science in **Applied Bioscience**

Thesis title: The identification of novel cys-loop receptor genes in *Dirofilaria immitis*

An oral defense of this thesis took place on October 17, 2023 in front of the following examining committee:

Examining Committee:

Chair of Examining Committee	Dr. Dario Bonetta
Research Supervisor	Dr. Sean Forrester
Examining Committee Member	Dr. Denina Simmons
Thesis Examiner	Dr. Holly Jones-Taggart

The above committee determined that the thesis is acceptable in form and content and that a satisfactory knowledge of the field covered by the thesis was demonstrated by the candidate during an oral examination. A signed copy of the Certificate of Approval is available from the School of Graduate and Postdoctoral Studies.

ABSTRACT

Dirofilaria immitis is a parasitic nematode responsible for canine heartworm disease. Currently, heartworm treatments rely primarily on a single drug class – the macrocyclic lactones – but anthelmintic resistance is emerging. Cys-loop ligand-gated ion channels are an untapped source for drug targets essential for nematode neurotransmission. This thesis presents the isolation and preliminary pharmacological characterization of three inhibitory *D. immitis* ion channels: GLC-2, GLC-4, and LGC-49. These genes are conserved across nematode species and expressed throughout the *D. immitis* life-cycle, as demonstrated by phylogenetic analysis and RT-qPCR. Dim-GLC-2 forms a monosodium L-glutamate (MSG) and L-glutamic acid sensitive homomeric channel, whereas the Dim-GLC-2/Dim-GLC-4 heteromeric channel shows reduced MSG current amplitude. The Dim-LGC-49 homomeric channel is responsive to cholinergic compounds. Homology modelling of homomeric channels highlights binding pocket residues which may interact with ligands. This research provides additional information on cys-loop receptors in parasitic nematodes crucial for understanding the action of potential new drugs.

Keywords: Heartworm; Cys-loop LGICs; Dirofilaria immitis; Anthelmintic resistance

AUTHOR'S DECLARATION

I hereby declare that this thesis consists of original work of which I have authored. This is a true copy of the thesis, including any required final revisions, as accepted by my examiners.

I authorize the University of Ontario Institute of Technology (Ontario Tech University) to lend this thesis to other institutions or individuals for the purpose of scholarly research. I further authorize University of Ontario Institute of Technology (Ontario Tech University) to reproduce this thesis by photocopying or by other means, in total or in part, at the request of other institutions or individuals for the purpose of scholarly research. I understand that my thesis will be made electronically available to the public.

The research work in this thesis that was performed in compliance with the regulations of Research Ethics Board/Animal Care Committee under Animal care certificate file number 16312.

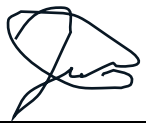

Jennifer S. Nichols

STATEMENT OF CONTRIBUTIONS

I hereby certify that I am the sole author of this thesis and that no part of this thesis has been published or submitted for publication. I have used standard referencing practices to acknowledge ideas, research techniques, or other materials that belong to others. Furthermore, I hereby certify that I am the sole source of the creative works and/or inventive knowledge described in this thesis.

ACKNOWLEDGEMENTS

I would like to first acknowledge Dr. Sean Forrester for the opportunity to pursue my graduate studies in his lab and for seeing my potential as an undergraduate student. The skills and knowledge I have gained while working under your supervision are invaluable and have helped me grow both as a researcher and a person. Thank you for always being available to support me through my studies. Your understanding, encouragement, and positive outlook have made working in your lab a wonderful and fulfilling experience.

To my committee member Dr. Denina Simmons, thank you for your time and support in the completion of my Master's degree. Your constructive feedback and suggestions are always appreciated. I am also grateful to Dr. Holly Jones-Taggart and Dr. Dario Bonetta for their roles on my defence examining committee.

I would like to thank my lab colleagues whom I have had the pleasure of meeting these past few years. First, thank you to Sierra for showing me practically everything about molecular cloning and electrophysiology. I appreciate the talks about podcasts and true crime, all the help you offered when troubleshooting the many problems related to electrophysiology, and just bouncing ideas around together. Thanks to Autumn, my desk buddy during my first year in the lab, for keeping me entertained with your chemistry and stories. To Amy, even though our time together in the lab was short, your presence was always warm and welcoming. Lastly, thank you to my undergraduate students Flavia, Devina, Praveen, and, indirectly, Vanessa for their help in the lab. Mentoring you was the most rewarding part of my graduate studies, and I am very fortunate to have met you all. I have enjoyed watching you grow as scientists and look forward to see what you will do next.

Finally, I want to thank my family and friends for their endless love and support. My mother, Anne, and Father, Steve, have been nothing but caring and encouraging these past few years. I would not have been able to achieve as much as I did without either of you. To Charlie, Doug, and Penny, thank you for lending an ear and always being by my side. To Makenzie, thank you for getting through not only my undergraduate studies but my graduate studies with me as well. Every step of the way, you encouraged me to keep going even when times were rough. You are my best friend, and I can't wait to see what happens next for us.

TABLE OF CONTENTS

LIST OF FIGURES

Chapter 1

Chapter 3

LIST OF ABBREVIATIONS AND SYMBOLS

Å	Angstrom (unit of distance measurement)
α	Greek symbol alpha
ACC	Acetylcholine-gated chloride channel; subunit annotation
Ace	*Ancylostoma ceylanicum*
ACh	Acetylcholine
β	Greek symbol beta
Bma	*Brugia malayi*
Carbachol (Car)	Carbamylcholine
Cbr	*Caenorhabditis brenneri*
cDNA	Complimentary DNA
Cel	*Caenorhabditis elegans*
Cq	Threshold cycle
cRNA	Copy RNA
Cys-loop	Cysteine-loop
Dim	*Dirofilaria immitis*
DOPE	Discrete optimized protein energy
EC_{50}	Half maximal effective concentration
ECD	Extracellular domain
GABA	Gamma-aminobutyric acid
GLC	Glutamate-gated chloride channel; subunit annotation
GluCl	Glutamate-gated chloride (channel)
Hco	*Haemonchus contortus*
ICD	Intercellular domain
L3/L4	Third/fourth-stage larvae
Lev	Levamisole chloride
LGC	ligand-gated channels; subunit annotation
LGIC	Ligand-gated ion channel

M1-M4	Transmembrane alpha helices 1-4
Mf	Microfilaria
ML	Macrocyclic lactone
MSG	Monosodium L-glutamate
nA	Nanoampere (Unit of electric current measurement)
nAChR	Nicotinic acetylcholine receptor
NRT	No reverse transcriptase
NTC	No template control
π	Pi
PAR	proline-alanine-arginine motif
PCR	Polymerase chain reaction
Ppa	*Pristionchus pacificus*
Pyr	Pyrantel citrate salt
RT-qPCR	Reverse transcriptase-quantitative polymerase chain reaction
Taq	*Thermus aquaticus*
TBE	Tris/Borate/EDTA
TEVC	Two-electrode voltage clamp
TMD	Transmembrane domain
X. laevis	*Xenopus laevis* (African clawed frog)

Chapter 1: Introduction and Literature Review

1.1 Introduction

Nematode parasitism is an increasing global veterinary concern. *Dirofilaria immitis* is a mosquito-borne parasitic nematode that interferes with the cardiovascular system of infected canines. Currently, *D. immitis* treatments include broad-spectrum anthelmintics, primarily macrocyclic lactones. The consistent misuse and overprescription of these drugs have resulted in the rise of drug resistance. Before *D. immitis* infections become impossible to treat, the development of new anthelmintics is essential. A superfamily of nematode receptors – the cysteine-loop ligand-gated ion channels (cys-loop LGICs) – include many potential drug targets. This thesis reports the initial identification and evaluation of novel cys-loop *D. immitis* receptors and contributes to our current knowledge of this class of receptors which is necessary for understanding drug action.

1.2 *Dirofilaria immitis*

A pathogenic helminth of high veterinary importance is the filarial nematode *D. immitis,* more commonly known as canine heartworm. *D. immitis* is an endoparasite responsible for causing the death of companion animals globally through canine heartworm disease. These worms reside within the circulatory system of infected animals, primarily within the heart and pulmonary arteries, where they feed off of nutrients in the host's bloodstream (Noack *et al.,* 2021). In dogs, symptoms of infection begin with coughing, general fatigue, and exercise intolerance, but, over time, can progress to extreme weight loss, shortness of breath, fainting, and hemoptysis – the coughing up of blood due to inflammation and lung tissue damage. In more advanced cases, the infection can become life-threatening due to large numbers of adult worms blocking blood flow

from the heart, leading to cardiovascular collapse and heart failure (Noack *et al.*, 2021). While dogs are the definitive host of *D. immitis*, infection can spread to less suitable hosts, including other canids, felids, and even humans. *D. immitis* causes pulmonary dirofilariasis in humans, characterized by the formation of pulmonary nodules around worms, and the disease can be asymptomatic or cause mild symptoms such as coughing, fever, and chest pain (Reddy, 2013). Although human infections are rare and cannot transmit from person to person, there is still the risk of zoonotic infections of *D. immitis* (Simón *et al.*, 2012). Considering the devastating symptoms of *D. immitis* caused infections in hosts and the present ability for zoonosis, efficient and effective heartworm treatments must be established to limit parasite spread.

1.3 The *D. immitis* infection cycle

Designing better heartworm treatments requires understanding which stages in the parasite transmission cycle anthelmintics act on. Like other filarial nematodes, *D. immitis* has no free-living life stage and is transmitted between hosts by an insect vector (Simón *et al.*, 2012). As depicted in **Figure 1.1**, there are six main stages to the *D. immitis* infection cycle in canines. It begins when a female mosquito takes a blood meal from an infected host and ingests circulating microfilariae (Mf), the earliest larval stage of heartworm. Within the intermediate host, the Mf migrate to the principal cells of the mosquito's renal organ in the abdomen, the Malpighian tubules (Sneed *et al.*, 2022). Here, the subsequent moults of Mf are temperature-dependent and require ambient temperatures of at least 14°C for maturation (Knight & Lok, 1998). Due to this, larvae may remain within the vector for as little as eight days or up to a month until Mf develop into the infective third larval stage (L3). These now infective larvae travel to the

mouthpiece of the mosquito, where they are deposited subcutaneously in a new mammalian host when the mosquito takes another blood meal. The L3 larvae moult into the fourth larval stage (L4) soon after infection – 3 to 12 days – and moult once more roughly 50 to 70 days post-infection to produce preadult worms that migrate towards the pulmonary artery and right chambers of the heart (Simón *et al.*, 2012). Here, worms mature to the adult stage approximately six months post-infection and can survive up to 10 years, feeding and mating to produce live young Mf that circulate in the peripheral bloodstream (Noack *et al.*, 2021). There is now potential for another female mosquito to ingest Mf and effectively restart the cycle. Considering heartworm treatment, the best anthelmintic would act on *D. immitis* at every life stage.

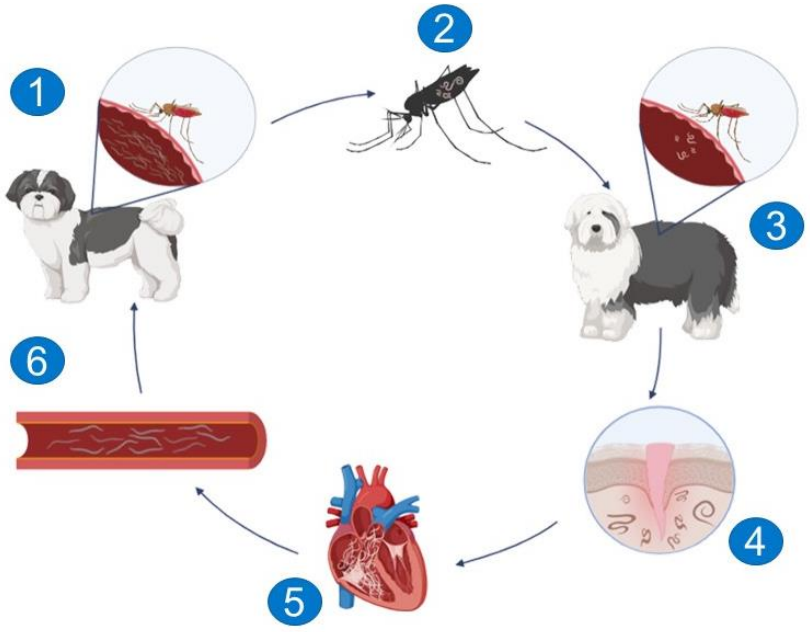

Figure 1.1 – The main stages of the *D. immitis* transmission cycle. (1) A mosquito takes a blood meal from a microfilaremic dog with an established heartworm infection. (2) The Mf moult into an infective L3 stage within the vector. (3) The mosquito transmits the infective larvae to a new host during a second blood meal. (4) L3 worms develop into the fourth-larval stage under the skin of the bite wound and migrate towards the pulmonary arteries and heart. (5) Adult worms establish themselves and mate within the cardiopulmonary system. (6) Mf are produced and released into host bloodstream, restarting the cycle. Figure was made in Biorender.

1.4 *D. immitis* prevalence and distribution patterns

While *D. immitis* is one of the most globally dominant canine parasite species, heartworm incidence in Canada varies by province. Nationwide, the prevalence of heartworm is 0.16%, which is substantially lower than the worldwide prevalence of 10.91% (Anvari *et al.*, 2020). This makes *D. immitis* infections rare throughout Canada when compared to other countries. However, heartworm is still endemic in several regions across the nation, with the majority of cases occurring in the southern parts of Manitoba, Quebec, and Ontario, where prevalence is 0.35%, 0.27%, and 0.12%, respectively (McGill *et al.*, 2019b). However, the most positive heartworm tests are reported in Ontario (McGill *et al.*, 2019b). Hyperendemic regions within the province include First Nations communities in the southeast and southwest, where prevalence was >15% for both areas (Jacobson *et al.*, 2020). Trends in *D. immitis* infections demonstrate that heartworm prevention and treatment should be a national and provincial priority.

Several factors influence the distribution patterns of *D. immitis* infections across Canada. Climate change is associated with the observed heartworm prevalence as it allows for prolonged periods of higher seasonal temperatures nationwide (McGill *et al.*, 2019a). This optimizes larval development within mosquitos to the infective L3 life stage and lets mosquitos extend the range of their habitat to introduce the parasite to new areas further north. In Southern Ontario, over 22 species of mosquitos can act as vectors for *D. immitis*, and the transmission season can begin as early as mid-May and last until the beginning of October (McGill *et al.*, 2019a). Since, generally, Southern Ontario is the first region to experience warmer temperatures in Canada and the last to experience cooler temperatures, this results in a lengthier transmission season for the parasite.

Ontario is also the province where the most heartworm testing occurs (McGill *et al.*, 2019a; McGill *et al.*, 2019b), which may explain why Ontario has the most positive tests, yet a lower heartworm prevalence when compared to Manitoba and Quebec. As for the hyperendemic regions in Ontario, factors such as limited access to veterinary care and cost of treatment likely contribute to heartworm prevalence (Jacobson *et al.*, 2020). The development of improved heartworm treatments and increased accessibility of these treatments will benefit dogs in Canada and globally.

1.5 Current heartworm treatments

D. immitis control depends heavily on synthetic and broad-spectrum anthelminthic drugs that result in worm death. No single medication is effective against every life stage of *D. immitis,* so the treatment of heartworm disease depends on the developmental stage of present worms. Currently, heartworm prevention in dogs is prioritized over heartworm treatment, which limits available options to eradicate established *D. immitis* infections. To improve upon current anthelmintics, one must first assess the benefits and drawbacks of each drug class used in heartworm prevention and treatment.

The primary drug classes used in *D. immitis* infection treatment are macrocyclic lactones, organic arsenical compounds, and antibiotics.

1.5.1 Macrocyclic lactones

The macrocyclic lactone (ML) drug class is the predominant drug class used in heartworm prevention and treatment and consists of two sub-groups: avermectins and milbemycins. The avermectins – including drugs such as ivermectin, abamectin, and selamectin – and the milbemycins – milbemycin oxime and moxidectin – have minor

structural differences, but the mechanism of action is the same for all (Noack *et al.*, 2021). The monthly administration of ML preventatives stops infections from becoming established. In invertebrates, MLs bind to the allosteric site of glutamate-gated chloride channels (GluCls) in nematode nerve cells and pharyngeal myocytes and either activate the channel directly or enhance the effect of natural GluCl agonists (Choudhary *et al.*, 2022). Increases in cell membrane permeability to anions results in cell hyperpolarization and worm paralysis, effectively killing L3 and L4 worms before they reach the pulmonary artery and mature to adulthood. The GluCls are only found in animals belonging to the phylum *Nematoda* or A*rthropoda* (Choudhary *et al.*, 2022), so off-target effects are limited in mammalian hosts. While regular dosing with MLs has proven to be efficacious in preventing the spread of *D. immitis* infections, they can only be used as a treatment for heartworm up to 60 days post-infection as it has little-to-no impact on mature adult worms (Bowman & Drake, 2017). Also, in the case of established infections, preventative drugs do not suppress circulating Mf in the blood, and many will survive despite encountering a macrocyclic lactone (Wolstenholme *et al.*, 2015). Whether exposing Mf or adult worms to ML preventatives, these drugs can select for ML-resistant worms, which can then be transmitted between dogs by insect vectors.

1.5.2 Organic arsenical compounds

Melarsomine dihydrochloride is an organic, arsenical compound and is the only adulticide approved to treat heartworm infections. The mechanism of action of melarsomine is not entirely understood, but it is believed to alter nematode glucose uptake and metabolism, modify the function and structure of the worm's intestinal epithelium, and inhibit the enzyme glutathione reductase (American Academy of

Veterinary Pharmacology & Therapeutics, 2008). Melarsomine is effective at killing worms from the young L4 to the adult life stages, but it is not approved for use in dogs with late-stage infections as there is a significant risk of pulmonary thromboembolism due to dead adult worms blocking the pulmonary arteries and heart chambers (Noack *et al.*, 2021). It is also an arsenic-based drug, and its use can be associated with severe neurological side effects (Bowman, 2012).

1.5.3 Antibiotics

The only antibiotic regularly used in heartworm treatments is doxycycline. Doxycycline does not act directly on *D. immitis* but rather on endosymbiotic bacteria of the *Wolbachia* genus found within the worms. *Wolbachia* bacteria are suggested to be required for correct larval development and embryogenesis of filarial worms, as well as for the long-term viability of adult worms (Simón *et al.*, 2012). Therefore, eliminating *Wolbachia* bacteria with doxycycline will effectively kill L3 and L4 worms and make adults more susceptible to adulticidal treatment. However, heartworm treatment with doxycycline lasts 1-3 months, and this treatment duration is often associated with severe gastrointestinal side effects and low host tolerance (Noack *et al.*, 2021). Co-administration of doxycycline with ivermectin and melarsomine enables a shorter and superior treatment regimen with microfilaricidal and adulticidal effects (Simón *et al.*, 2012). This combination chemotherapy approach, while effective and efficient, does not erase the adverse effects and limitations associated with the existing protocols for heartworm treatment.

1.6 The rise of anthelmintic resistance in *D. immitis*

Drug resistance can arise from under-dosing, inappropriate administration, or over-prescription of anthelminthic drugs. Heartworm treatments have a gap in effectiveness, known as the susceptibility gap, as certain life stages of *D. immitis* are not entirely susceptible to treatment by either MLs or melarsomine (Bowman & Drake, 2017). If Mf are exposed to MLs or adulticides and live long enough to reproduce, the probability of resistance emerging increases. All available heartworm preventatives belong to the ML drug class. Since heartworm chemotherapy relies so heavily on the use of MLs, the occurrence of resistance against one preventative drug makes the development of cross-resistance extremely likely due to the structural similarities of the drugs used. Reports of confirmed resistance and loss-of efficacy of the preventatives against specific strains of *D. immitis* raise serious concerns about the future of heartworm control (Bowman, 2012; Geary *et al.*, 2011). In addition, present treatments can be expensive and lengthy depending on the advancement of infection, which does not bode well for infected dogs in low-income communities or shelters, where heartworm is more prevalent and infected canines act as reservoirs for the parasite (Jacobson *et al.*, 2020). For these reasons, it is imperative to characterize novel drug targets for improved anthelminthic treatments.

1.7 The nematode nervous system

Many current anthelmintics available target the nematode nervous system. The nervous system of nematodes is relatively simple and well-conserved across nematode species and contains only about 300 individual neurons (Wolstenholme 2011). While anatomically straightforward, the nematode nervous system is chemically complex, as

many transmitters and receptors are not found in mammals. LGICs are integral membrane proteins within the nervous system that allow for the transmittance of synaptic messages between neurons and at neuromuscular junctions (Choudhary *et al.*, 2022). In nematodes, behaviours such as reproduction, locomotion and feeding are all controlled by LGICs. Upon agonist binding, the LGIC permits ion flux across the cell membrane, producing either an excitatory or inhibitory response depending on the receptor activated (Choudhary *et al.*, 2022). Anthelmintics which target ion channels quickly impede synaptic transmission by causing prolonged cell depolarization or hyperpolarization due to cation or anion influx, respectively (Wolstenholme 2011). Therefore, novel neuroactive anthelmintics have the potential to be broad-spectrum and exert less severe side-effects to mammalian hosts while still effectively killing parasitic nematodes.

1.8 Cysteine-loop ligand-gated ion channels

The cys-loop LGICs are a large and diverse superfamily of receptors that show promise as novel anthelmintic targets. The cys-loop LGICs are ionotropic receptors necessary for intracellular communication and neuronal signalling in mammals and invertebrates, and include the nicotinic acetylcholine receptors (nAChRs), serotonin receptors, gamma-aminobutyric acid (GABA) receptors, and glycine receptors (Thompson *et al.*, 2010). However, compared to mammalian receptors, nematodes contain a broader repertoire of individual receptor types which respond to a much larger array of agonists. Many of these receptors play an essential role in the survival of the worm (Thompson *et al.*, 2010). For some nematodes, including the free-living *Caenorhabditis elegans* and the parasitic *Haemonchus contortus*, the cys-loop LGIC family is quite large, containing 102 and 64 genes which encode cys-loop receptor

subunits, respectively (Jones & Sattelle, 2008; Laing *et al.*, 2013). However, in *D. immitis,* only 24 genes encode cys-loop receptor subunits (Coghlan *et al.*, 2019).

While there is variation in agonist response and function between cys-loop LGICs, the general structure of each receptor is the same (Thompson *et al.*, 2010; Choudhary *et al.*, 2022). The cys-loop receptors consist of five subunits organized pseudo-symmetrically around an ion-conducting pore (**Figure 1.2A**). Cys-loop receptors are named after the distinctive and conserved cys-loop motif present in the extracellular domain of a subunit, consisting of a disulphide bond between two cysteine residues 13 amino acids apart (**Figure 1.2B**). This structure plays an integral role in receptor assembly and the gating of the channel pore (Jones & Sattelle, 2008). Each subunit of a cys-loop receptor is composed of three domains: (1) the extracellular domain (ECD), which contains the N-terminus ligand binding domain, (2) the transmembrane domain (TMD), composed of four hydrophobic alpha-helices (M1-M4), and (3) the small intracellular domain (ICD) which links the receptor to the cytoskeleton and plays a role in channel conductance (**Figure 1.2B, Figure 1.3**). The M2 helix lines the channel pore and conveys ion specificity. Identical subunits or homologous subunits can combine to form homomeric channels or heteromeric channels, respectively (Choudhary *et al.*, 2022). The different combinations of subunits can impact the functional and pharmacological properties of the channel. Through agonist binding, these receptors increase the cell membrane permeability to specific ions, while antagonist binding reduces permeability by opposing the action of the agonist (Thompson *et al.*, 2010).

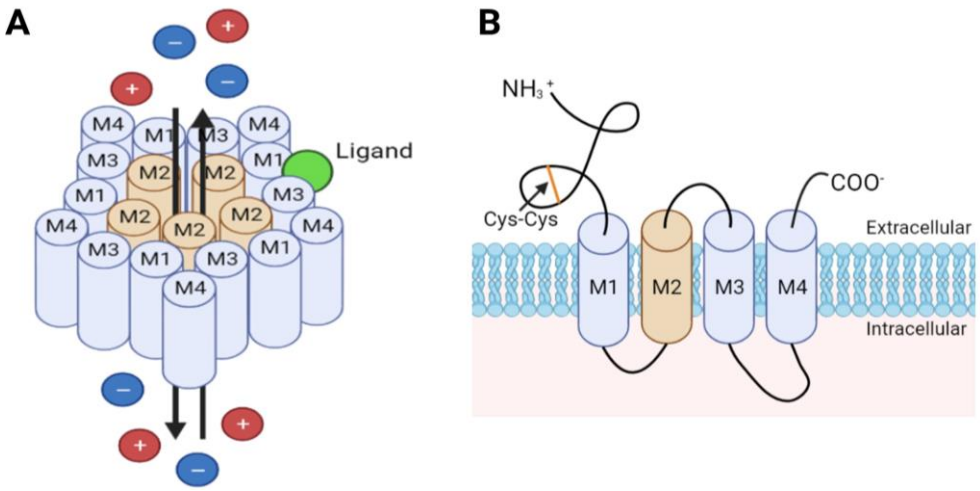

Figure 1.2 – The topology and structure of cys-loop LGICs. (**A**) A complete pentameric, ion-conducting cys-loop LGIC. The M2 helix of each subunit lines the central pore. Ligand binding induces a conformational change of the protein to allow for ion flux. (**B**) The structure of an individual cys-loop LGIC subunit highlighting the N-terminal extracellular domain, the transmembrane alpha helices (M1-M4), cys-loop, and intracellular domain. Figure was made in Biorender.

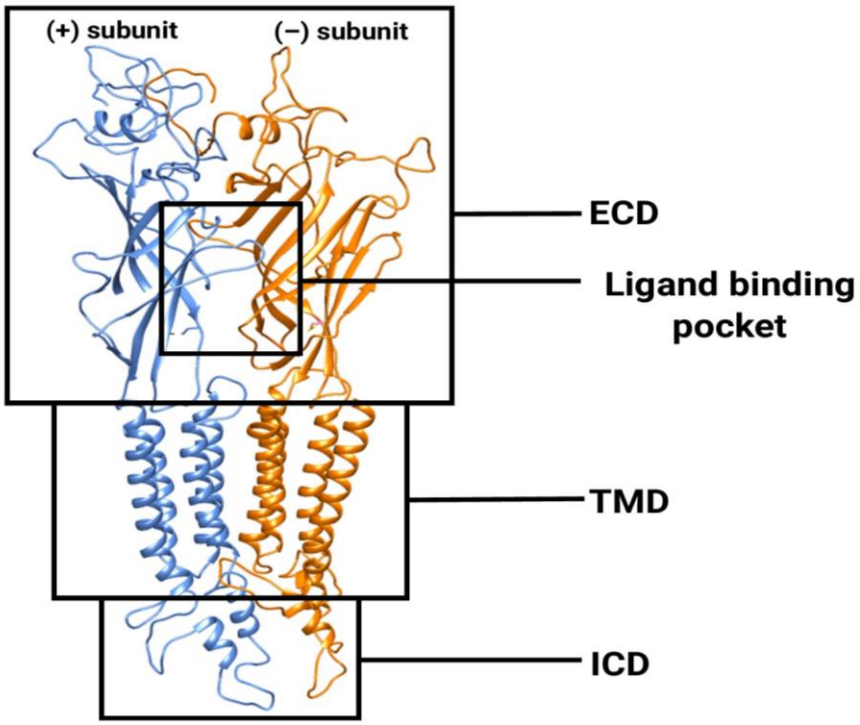

Figure 1.3 – Molecular model of a representative cys-loop receptor subunit dimer. The image shows the principal (+) and complimentary (-) subunit interface. ECD = extracellular domain. TMD = transmembrane domain. ICD = intracellular domain. The ligand binding domain is found between the (+) and (–) subunits in the ECD.

1.9 The cys-loop receptor binding pocket

Molecular recognition depends on reversible non-covalent interactions between the ligand and receptor within the binding pocket. Within a cys-loop receptor, the binding pocket is in the ECD at the interface of two adjacent subunits: the principal (+) subunit, which contributes binding loops A-C, and the complementary (-) subunit, which contributes binding loops D-G (**Figure 1.4**). Here, the sidechains of the amino acid residues on the binding loops allow for ligand binding through the formation of various types of non-covalent bonds (Thompson *et al.*, 2010).

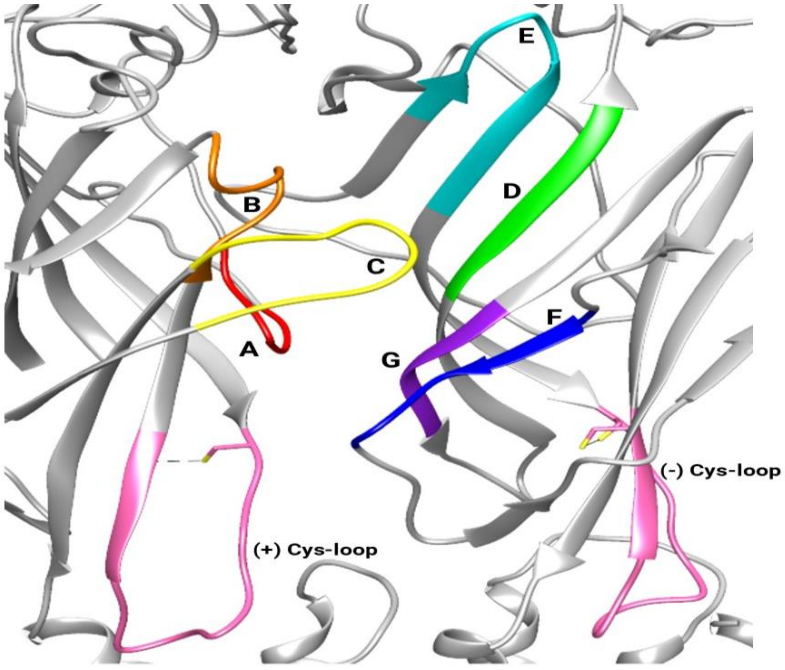

Figure 1.4 – The seven binding loops (A-G) and characteristic cys-loops of a cys-loop LGIC binding pocket.

The types of non-covalent interactions present within the binding pocket depend on the functional groups of the ligand and surrounding amino acid side chains. First are electrostatic forces between atoms, which can be attractive if the atoms carry opposite charges or repulsive if they carry the same charge (Chen & Kurgan, 2009). Amino acids

with charged side chains at physiological pH include the cationic arginine, lysine, and histidine, and the anionic aspartic acid and glutamic acid. The distance and subsequent strength of these electrostatic attraction and repulsion forces depend on variables such as the size of atomic radii but often fall within 3.5Å (Chen & Kurgan, 2009). Additionally, electrostatic interactions can occur between the aromatic rings of amino acid side chains (phenylalanine, tryptophan, and tyrosine) and ions known as cation-π interactions (Infield *et al.*, 2021). The aromatic ring involved in the interaction provides a surface of negative electrostatic potential that stabilizes cations. Cation-π bonds play an important role in agonist binding, and for these interactions to exist, the cation must be directly aligned over the center of the aromatic ring and be no more than 6Å away (Infield *et al.*, 2021). Other interactions within the binding site include hydrogen bonds, which are relatively weak attractions between a hydrogen atom bound to a highly electronegative donor atom (oxygen, nitrogen, or fluorine) and another highly electronegative acceptor atom. Typically, they form at distances of no greater than 3.5Å between the donor and acceptor atoms (Chen & Kurgan, 2009). Ionic hydrogen bonds are a special class of stronger hydrogen bonds that form between a cationic or anionic hydrogen donor atom and a neutral hydrogen acceptor atom (Meot-Ner, 2005). Finally, van der Waal forces are weak general attractive forces between molecules due to the temporary fluctuation in electron density. Van der Waal forces are the most common protein-ligand interactions and typically occur within an intramolecular distance of 4.0Å or less in binding pockets (Chen & Kurgan, 2009). $\Delta Cq = Cq\ (GOI) - NF$

The relative strengths of these interactions cannot accurately be ranked. It is important to note that many factors influence bond strength, such as the size and

geometry of interacting molecules, the specific atoms interacting, the distance between atoms, and the surrounding environment (Chen & Kurgan, 2009). These interactions also occur simultaneously, which can lead to synergistic effects or interaction cancellation, further complicating any ranking. Understanding which non-covalent interactions occur within a cys-loop receptor binding site can help identify residues that may be important when designing novel anthelmintics.

1.10 Groups of cys-loop LGICs

The superfamily of cys-loop receptors is divided into subgroups based on sequence homology. Subunits belonging to the same group can share many qualities, such as ligand specificity, location within the nematode, and ion specificity (Jones & Sattelle, 2008). Invertebrates express a greater range of inhibitory cys-loop receptor types than vertebrates including GABA-, dopamine-, serotonin-, and tyramine-gated chloride channels. There are two additional groups that are the focus of this thesis: the AVR-14 and ACC-1 groups, which are glutamate- and acetylcholine-gated chloride channels, respectively.

1.10.1 The AVR-14 group

The AVR-14 group of cys-loop receptors includes six subunits first identified in *C. elegans – glc-1, glc-2, glc-3, glc-4, avr-14, avr-15* –which make up the GluCls targeted by the ML drug class (Jones & Sattelle, 2008). However, in *Brugia malayi*, a parasitic filarial nematode belonging to the same clade as *D. immitis,* only four subunits have been identified based on homology searching – *glc-2, glc-4, avr-14A,* and *avr-14B* (Williamson *et al.*, 2007) – which suggests the available subunits to be targeted by anthelmintics in *D. immitis* may be more limited when compared to free-living

nematodes. Channels belonging to this invertebrate-specific grouping of receptors are located in pharyngeal muscles, reproductive tissues, and motor and sensory neurons of nematodes (Choudhary *et al.*, 2022). The natural ligand of the AVR-14 receptors is L-glutamate, which, at physiological pH, has three charged functional groups available for receptor binding (**Figure 1.5A**). The channels are chloride-selective and upon activation, the anion influx results in muscle relaxation (Choudhary *et al.*, 2022). Anthelmintic action, therefore, relies upon the prolonged activation of these channels due to high receptor binding affinity to cause worm paralysis and death. For *D. immitis*, the pharmacological properties of the GluCls remain largely unknown despite being the targets of the most widely-used drug class for heartworm treatment. Therefore, further exploration into the structure and ligand sensitivity of *D. immitis* GluCls can reveal important information on the action of anthelmintics

1.10.2 The ACC-1 group

A unique group of channels is the ACC-1 family of receptors which includes eight subunits – *lgc-46, lgc-47, lgc-48, lgc-49, acc-1, acc-2, acc-3, and acc-4* (Jones & Sattelle, 2008). The expression location of individual subunits varies within a nematode, but the ACC-1 channels are expressed throughout the nervous system. Acetylcholine activates channels belonging to the ACC-1 family, similar to the nAChRs, and the molecule possesses a cationic quaternary amine and an ester functional group available for binding (**Figure 1.5B**). However, the ACC-1 receptors are chloride-selective and more similar to glycine receptors than nAChRs (Choudhary *et al.*, 2022). Since the ACC-1 channels are not present in mammals, possess distinct pharmacological profiles, and are expressed in vital nematode tissues, they have great potential to be used as future

anthelmintic targets (Putrenko *et al.*, 2005). In *D. immitis*, the ACC-1 group of receptors have not been explored as a source of drug targets despite obvious potential.

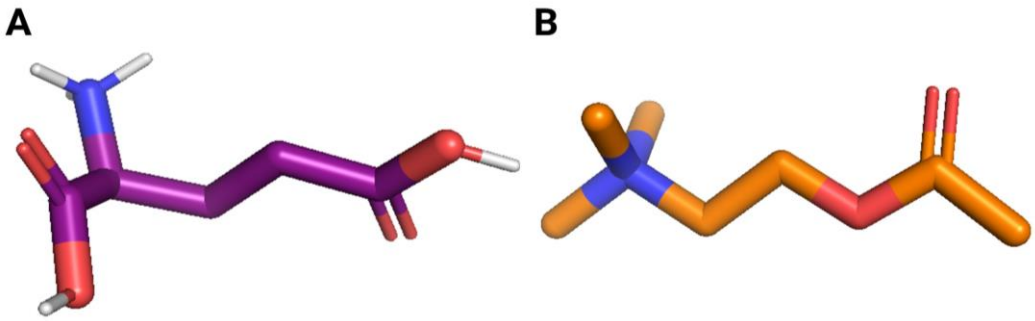

Figure 1.5 – The structures of the natural ligands for GluCl and ACC-1 channels (**A**) L-glutamate and (**B**) acetylcholine. Blue atoms represent nitrogen, red atoms represent oxygen, and white atoms represent hydrogen. Only polar hydrogen atoms are shown.

1.11 Rationale and objectives

Considering recent resistant trends in heartworm prevention and the limited options for treatment, there is an immediate need for novel anthelmintics. Cys-loop LGICs from other nematodes have been well-studied, but the characterization of *D. immitis* orthologues is lacking. There is untapped potential for novel drug targets that can lead to improved heartworm treatments in the future, but first, it is necessary to isolate and establish a pharmacological profile for the receptors. Therefore, this thesis aims to identify and preliminarily characterize expressed cys-loop receptor genes in *D. immitis*. Five objectives contribute to achieving this overarching goal:

1. Screen all 24 cys-loop encoding genes to determine which, if any, are expressed in different life stages of *D. immitis*. Genes highly expressed in the examined life stages will be further analyzed as they may be important for the biology of the parasite.

2. Isolate and phylogenetically analyze candidate gene sequences to confirm the gene is present and conserved across nematode species as this will identify an anthelmintic target that has broad-spectrum potential.
3. Evaluate the life stage expression of candidate genes. If the receptor is significantly expressed in given *D. immitis* life stages, it likely has a high physiological importance and will result in lethal effects if activated.
4. Clone the candidate genes into the *Xenopus laevis* oocyte expression vector pGEMHE to perform an initial pharmacological characterization of the receptors through two-electrode voltage clamp (TEVC) electrophysiology.
5. Enhance receptor structure understanding of the candidate receptors through computational homology modelling and ligand docking. This will highlight potentially important amino acid residues within the binding site of the receptor that allow for ligand recognition.

Chapter 2: Methods

2.1 RNA extraction and cDNA synthesis

Adult female, L3, and Mf total RNA were received from BEI resources (Virginia, USA). Frozen *D. immitis* adult male and female worms were obtained from BEI Resources and total RNA was isolated using and TRIzol (Invitrogen, California, USA) and sample homogenization. Complementary DNA (cDNA) was synthesized for all life stages using the Quantitect Reverse Transcriptase kit (Qiagen, Dusseldorf, Germany), using a unique 3' oligo-dT anchor primer with the following sequence: (5′CCTCTGAAGGTTCACGGATCCACATCTAGATTTTTTTTTTTTTTTTVN3′); [where V is either A, C, or G and N is either A, C, G, or T] (Weston *et al.*, 1999).

2.2 Gene screening and gene isolation

The initial screening of candidate genes began with assessing the expression of 20 cys-loop genes in *D. immitis* from the Mf, L3, and adult female life stages. Primers for partial sequence isolation for cys-loop LGIC genes were designed based on predicted scaffold gene sequences provided by Coghlan *et al.* (2019) as part of the International Helminth Genomes Consortium. To screen for candidate genes with adequate expression, initial end-point polymerase chain reactions (PCRs) were performed with *Taq* DNA polymerase (2 min 95°C, [15 s 95°C, 15 s --°C, 15 s 72°C] × 40 cycles, 3 min 72°C, with "--" denoting a primer pair-specific annealing temperature) to isolate fragments ranging from 200-300bp. All PCR products were run on 1% agarose gels, and several that produced amplicons of expected sizes were subsequently cloned into pGEM®-T easy sequencing vectors (Promega, Wisconsin, USA) and sent for sequencing through Genome Quebec (Nanuq, Quebec, CA). The screening of partial fragments revealed 15

genes expressed to varying degrees in at least one of the life stages examined. Three candidate genes selected for further study based on confirmed partial sequences and their expression in the adult female, L3, and Mf life stages were GLC-2, GLC-4, and LGC-49.

Using the predicted gene scaffold sequences, a bioinformatic screen was performed with the NCBI software BlastX (https://blast.ncbi.nlm.nih.gov/) to identify orthologues from closely related nematode species within the same nematode clade, primarily *Brugia malayi*. Based on nucleotide alignments and predicted start and stop codons from the orthologous sequences, primers specific for the hypothesized 5' and 3' end of the complete genes were designed within the scaffold sequence with restriction sites, and five random nucleotides were added upstream of the restriction site to improve enzyme cutting efficiency. Amplicons were restriction cloned into pGEMHE *Xenopus* expression vectors for downstream use (Zhang *et al.*, 2008). The confirmed sequences were analyzed using SignalP6.0 (https://biolib.com/DTU/SignalP-6/) to confirm the presence of a signal peptide and cleavage site and DeepTMHMM (https://dtu.biolib.com/DeepTMHMM) to confirm the presence of four TMDs.

2.3 Phylogenetic analysis

Cloned protein sequences from cDNA were used to search the NCBI protein database (http://blast.ncbi.nlm.nih.gov/) for other nematode gene sequences with high similarity for phylogenetic analysis. All sequence alignments were produced using Clustal Omega, and a phylogenetic tree was created using NGPhylogeny (https://ngphylogeny.fr) based on maximum likelihood with 100 bootstrap repetitions. Only gene regions highly conserved between species were used to generate the

phylogenetic tree. *H. contortus* LEV-1, a nAChR gene from a clade V nematode, was used as an outgroup.

2.4 Semi-quantitative end-point PCR

All RNA concentrations between the life stages examined were standardized prior to cDNA synthesis. Standard end-point PCR was executed using *Taq* DNA polymerase and primers specific to the 5' and 3' ends of GLC-2, GLC-4, and LGC-49. Reactions were performed in triplicate using cDNA from the adult male, adult female, L3, and Mf life stages. PCRs run with primers specific to the housekeeping gene β-tubulin were used as positive controls, and no reverse transcriptase (NRT) reactions were used as negative controls.

Resulting amplicons (PCR bands) were visualized under ultra violet (UV) illumination using ethidium bromide-stained 1% agarose gels made with Tris/Borate/EDTA (TBE) and the Axygen® gel documentation system (Corning, New York, USA). The TBE buffer was not reused between electrophoresis runs to avoid additive effects of ethidium bromide. ImageJ software was used to measure band density following the steps outlined by Antiabong *et al.* (2016). In short, the florescence signal of the gene of interest was measured and then normalized to that of the positive control. A heatmap was generated using the mean percent expression of each gene compared to the control using Heatmapper software (http://www.heatmapper.ca/).

2.5 Real-time quantitative PCR (RT-qPCR)

All RNA concentrations were standardized to a starting 852ng/ul for each cDNA synthesis reaction following the protocol described in **section 2.1** for the adult female, adult male, and Mf life stages. An initial 1:4 dilution was performed to get a starting

DNA concentration of 10.65ng/ul. This was then diluted in a 5-fold dilution series to make six separate DNA dilutions for points on the standard curve. The cDNA was stored at −20 °C until use.

Gene-specific primers were designed with the following criteria: length (20 to 27-mer), GC percentage (30-70%), melting temperature of approximately 60°C, an amplicon size ranging from 90-200bp, and at least one primer of the set spanning an exon-exon junction. Two endogenous control genes, GAPDH and DITPH, were selected based on their previous validation as reference genes (Thompson, 2016; (Vandesompele *et al.*, 2002). Additional primer information is available in **A1**. The optimization of primer concentrations and annealing temperatures were done prior to performing qPCR experiments. All standard curves, primer amplification efficiencies and linearity values were generated using CFX Manager software (Bio-Rad, California, USA). For each primer set, efficiency was determined using the standard curve made from six 5-fold serial dilutions of cDNA using the formula: E (%) = (10[-1/slope]-1) x 100.

Amplification was carried out in a CFX Connect Real-Time System (Bio-Rad, California, USA) using the following PCR protocol: 3min 95°C, [10s 95°C, 30s 55°C, 15s 72°C] x 40 cycles. RT-qPCR amplifications for all genes were carried out using 1µL of diluted cDNA template, 5µL of SsoAdvancedTM Universal SYBR® Green Supermix (Bio-Rad, California, USA), 1µL of forward and reverse primer, and 3µL of DNase/RNase free water for a final reaction volume of 10µL. Each qPCR plate contained a NRT and a no template control (NTC) to ensure there was no formation of secondary structures or DNA contamination. The amplification of a single product was confirmed

by melting curve analysis and gel electrophoresis. Isolated fragments were cloned, and sequences were confirmed by Genome Quebec (Nanuq, Quebec, CA).

Relative gene expression analysis was performed on three biological samples for each examined life stage that were assayed in technical triplicates. The technical replicate average threshold cycle (Cq) for each biological replicate was used in data analysis. Quantitative gene expression for the gene of interest was normalized to the arithmetic mean expression levels of both reference genes. A two-way analysis of variance (ANOVA) was used to evaluate if the Cq values for the biological replicates differed significantly for each gene of interest between all three life stages examined. ANOVA tests that gave a significant p value ($p < 0.001$) were followed with a post-hoc Tukey's honest significant difference test to determine which two life stages showed significantly different ($p < 0.001$) relative gene expression.

2.6 Expression in *X. laevis* oocytes

pGEMHE *Xenopus* expression vectors containing the complete gene sequence for GLC-2, GLC-4, or LGC-49 were linearized using the restriction enzyme NheI (New England Biolabs, Massachusetts, USA) to be used as template in *in vitro* copy RNA (cRNA) synthesis reactions with the mMESSAGE mMACHINE T7 Transcription Kit (Ambion, Texas, USA). All cRNA solutions were diluted with DNase/RNase free water to achieve a standard concentration for injection.

Any procedure involving the use of laboratory animals followed the guidelines provided by the University of Ontario Institute of Technology Animal Care Committee and the Canadian Council on Animal Care. Adult female *Xenopus laevis* frogs were supplied by Nasco (Fort Atkinson, Wisconsin, USA). The frogs were kept in a climate-

controlled (18°C), light-cycled room and were fed and cleaned regularly. To perform oocyte removal, *X. laevis* were anesthetized using 0.15% 3-aminobenzoic acid ethyl ester methanesulphonate salt (MS-222) [Sigma-Aldrich, Ontario, CA] brought to pH 7 with sodium bicarbonate, $NaCHO_3$. A portion of the frog ovary was removed, and sections of the lobe were defolliculated with OR-2, calcium-free oocyte ringer's solution [82 mM NaCl, 2 mM KCl, 1 mM MgCl2, 5 mM HEPES pH 7.5 (Sigma-Aldrich)] and 2mg/mL collagenase-II (Sigma-Aldrich). The oocytes were incubated in the solution for 30 min at room temperature under agitation and then rinsed with ND96 solution (96 mM NaCl, 2 mM KCl, 1 mM $MgCl_2$, 1.8 mM $CaCl_2$) to remove collagenase. Oocytes were incubated in ND96 supplemented with 50μg/mL gentamycin and sodium pyruvate for 1hr at 18°C before injection. Only stage V and VI oocytes were chosen for cRNA injection. Each oocyte was injected with 50nL (0.5ng/μL) of cRNA using the Drummond Nanoject II microinjector (Pennsylvania, USA) and incubated in supplemented ND96 at 18°C. Oocytes expressing Dim-GLC-2 and Dim-GLC-4 heteromeric channels were co-injected with equal concentrations of both genes (0.25ng/μL). Electrophysiological recordings were performed between 48h and 96h post-injection.

2.7 Electrophysiological recordings

To pharmacologically characterize the expressed ion channels, TEVC electrophysiology was executed using the Axoclamp 900A voltage clamp (Molecular Devices, California, USA). Glass electrodes were created using a P-97 Micropipette Puller (Sutter Instrument Co., California, USA). Electrodes were backfilled with 3M KCl and contained Ag|AgCl wires to connect each electrode to the head-stage. Ligand solutions were perfused over oocytes using the RC-1Z recording chamber (Warner

Instruments Inc., Connecticut, USA). Oocytes were then washed with ND96 recording buffer to remove residual ligands until a steady baseline was reached. Electrophysiological trace data was analyzed using Clampex Software v10.2 (Molecular Devices), and dose-response graphs were created using Graphpad Prism Software v5.0 (California, USA). The half maximal effective concentration (EC_{50}) values for LGC-49 and GLC-2 were determined by dose-response curves fitted to the equation:

$$I_{max} = \frac{1}{1 + (\frac{EC_{50}}{[D]})^{h}}$$

Here, *Imax* is the maximal response, EC_{50} is the ligand concentration required to elicit 50% of the maximal response, [D] is the ligand concentration, and *h* is the Hill slope coefficient. With the above equation, GraphPad Prism fits a sigmoidal curve with a variable slope to the data. Agonist dose-response curves were normalized to their individual *Imax* responses.

For LGC-49 pharmacological characterization, the following compounds were used: acetylcholine chloride (acetylcholine), carbamylcholine chloride (carbachol), levamisole hydrochloride (levamisole) [Sigma-Aldrich], and pyrantel citrate salt (pyrantel) [Santa Cruz Biotechnology, Texas, USA]. For the GluCls, the following compounds were used in pharmacological analysis: enantiopure monosodium L-glutamate (MSG) [Toronto Research Chemicals, Ontario, CA] and L-glutamic acid [Sigma-Aldrich]. L-glutamic acid solutions were pH adjusted to match the pH of the MSG solutions using sodium bicarbonate ($NaHCO_3$). Un-injected oocytes were used as a negative control.

2.8 *In silico* homology modelling and computational agonist docking

To analyze the binding pocket structure of the cloned subunits, dimer models were produced using the amino acid sequences of GLC-2 and LGC-49. Crystal structure templates with the highest sequence similarities with the genes of interest were obtained from SwissProt database (Swiss Institute of Bioinformatics, Switzerland). The *Danio rerio* alpha-1 glycine receptor (3JAD) template was used to model LGC-49 (Kumar *et al.*, 2020), and for the GLC-2, the crystal structure for a *C. elegans* glutamate-gated chloride channel α-subunit (3RIA) was used (Hibbs & Gouaux, 2011). All models were generated using automated scripts with MODELLER v10.3. The most energetically favourable model with the lowest discrete optimized protein energy (DOPE) score was selected for computational agonist docking.

Ligands in their energy reduced form were obtained from PubChem. The binding sites of the dimers were prepared for ligand docking using AutoDock Tools (Morris *et al.*, 2009). AutoDock Vina was used to simulate the docking of the ligand, and the version with the best binding affinity was chosen to be examined further (Trott & Olson, 2010). In the case of GLC-2, the version with an L-glutamate orientation that most closely resembled the published version was also used for comparison (Hibbs & Gouaux, 2011). Chimera v1.6.1 (Pettersen *et al.*, 2004) was used to determine the distance between the amino acid residues of the binding pocket and the docked ligands and for the generation of figures. The binding site simulation only included amino acid residues that had at least one non-hydrogen atom within 4.0Å of the ligand's non-hydrogen atoms as this distance encompasses any significant non-covalent interactions possibly present. The

distance parameter was extended to 6Å when examining potential cation-π interactions with aromatic residues. All residue-ligand interactions were considered independent.

Chapter 3: Results

3.1 Isolation of GLC-2, GLC-4, and LGC-49

The full-length sequences for GLC-2 and GLC-4 consisted of 1332 and 1545 nucleotides, respectively, encoding proteins of 443 and 514 amino acids, respectively. Both sequences included the hallmark cys-loop, all seven binding loops, and four transmembrane domains (**Figure 3.1**). A signal peptide and cleavage site, between residues Ala37 and Arg38 in GLC-4 and residues Ser20 and Thr21 in GLC-2, were found in both sequences. The sequence of Dim-GLC-4 is 68% similar to Cel-GLC-4 and 69% to Bma-GLC-4. Dim-GLC-2 has 66% sequence similarity with Cel-GLC-2 and a higher percent similarity of 89% with Bma-GLC-2. An adenine to guanine point-mutation was identified in the cloned adult male GLC-4 sequence, which changed an isoleucine to a methionine at position 21, as highlighted in **Figure 3.1**. The location of the point mutation is outside of the binding loops and TMDs, so this mutation is unlikely to impact ligand binding or receptor formation, but should be noted nonetheless. However, the conversion of an isoleucine to a methionine at this position does increase the predicted likelihood of the signal peptide and cleavage site by 3%.

The protein coding sequence for Dim-LGC-49 consisted of 1386bp and encodes a protein of 461 amino acids. The characteristic cys-loop, all extracellular binding loops and TMDs, and a signal peptide and cleavage site between residues Ala22 and Asp23 were all identified in the sequence. A PAR motif at the beginning of Dim-LGC-49 M2 indicates the channel formed by this subunit is anion selective (Jensen *et al.*, 2002). At the amino acid level, LGC-49 exhibits 65%, 67%, 67%, and 69% sequence similarity with orthologues from *Caenorhabditis brenneri* (Cbr), *Ancylostoma ceylanicum* (Ace), *C.*

elegans, and *Pristionchus pacificus* (Ppa), respectively. When aligned to other protein orthologues, the highly conserved regions observed are the binding loops and TMDs (**Figure 3.2**).

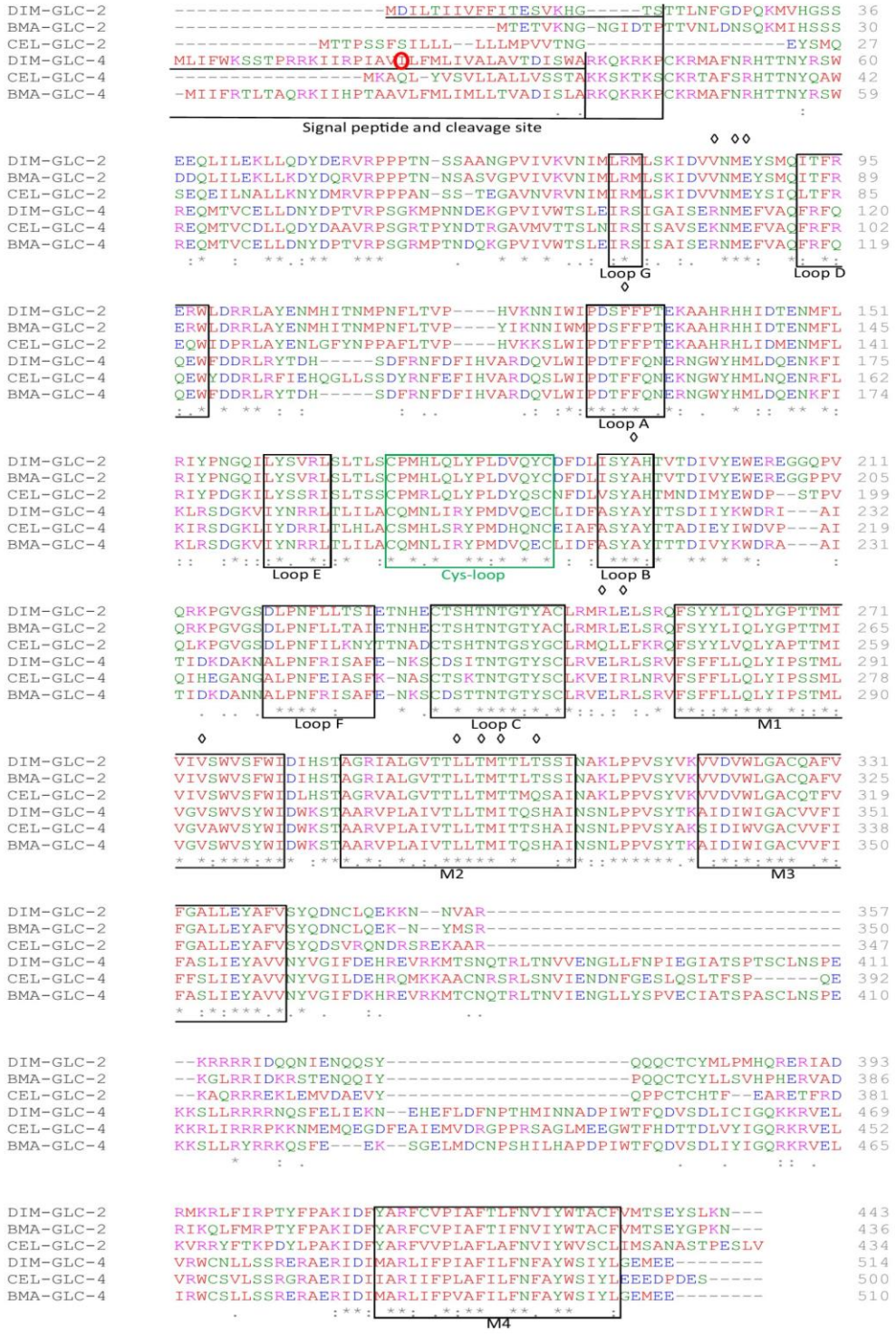

Figure 3.1 – *D. immitis* GluCl protein sequence alignment with GLC-2 and GLC-4 orthologues from *C. elegans* (Cel) and *B. malayi* (Bma). Important regions such as the signal peptide and cleavage site, binding loops (A-G), the characteristic cys-loop, and all transmembrane domains are indicated. The GLC-4 male point mutation is circled in red. (*) indicates identity, (:) indicates similarity, and (◊) indicates a residue which was identified to play a role in ligand binding, as per the homology models.

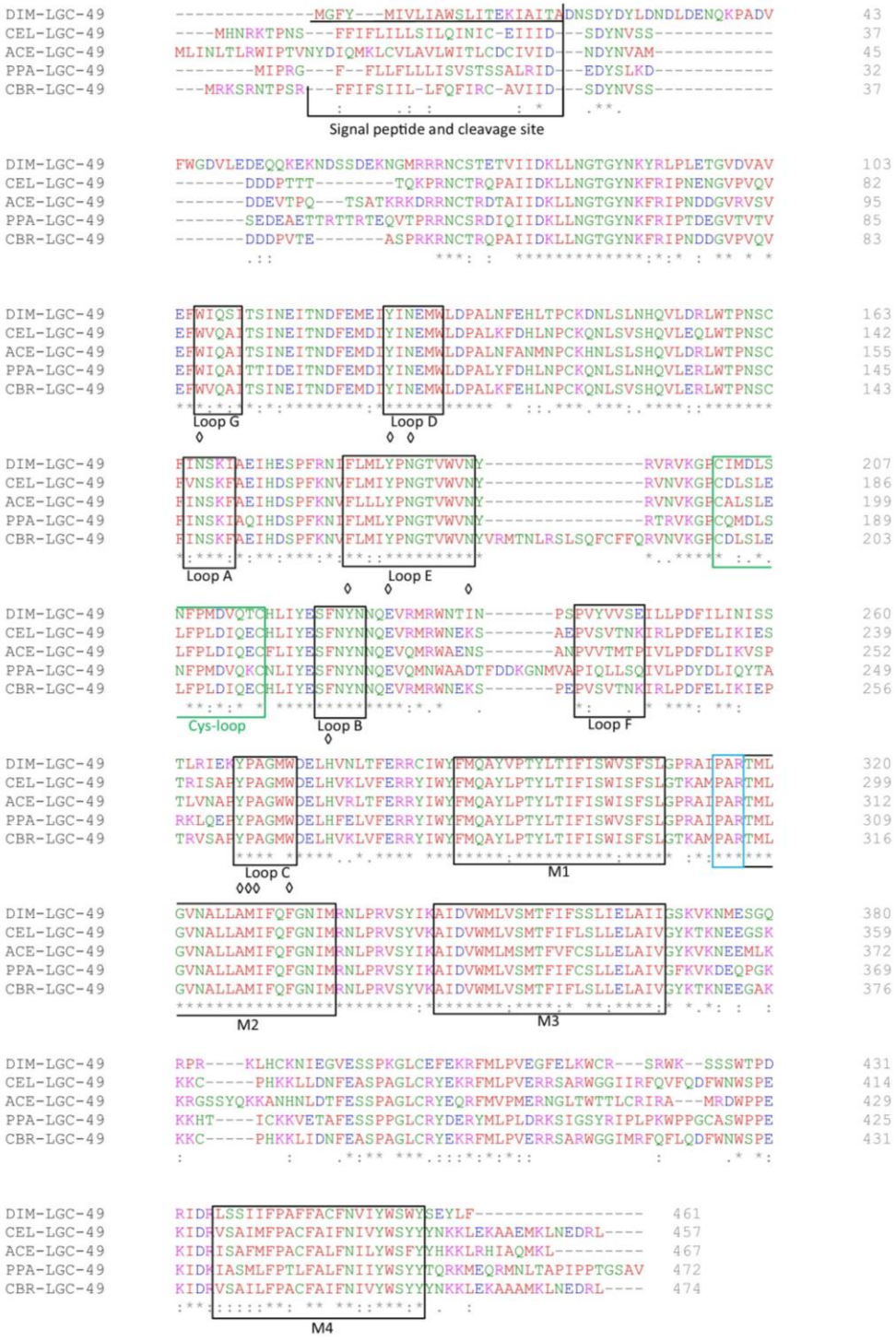

Figure 3.2 – Dim-LGC-49 protein sequence alignment with LGC-49 orthologues. Important regions such as the signal peptide and cleavage site, binding loops (A-G), the cys-loop, and all transmembrane domains are indicated. The M2 PAR motif is highlighted in blue (*) indicates identity, (:) indicates similarity, and (◊) indicates a residue which was identified to play a role in ligand binding, as per the homology models.

3.2 Phylogenetic analysis

The phylogenetic analysis of cloned *D. immitis* genes shows that the subunit proteins are conserved across nematode clades (**Figure 3.3**). Dim-LGC-49, Dim-GLC-2, and Dim-GLC-4 all group separately with their orthologous proteins with high bootstrap confidence values. The GluCls branch off together first from genes belonging to the ACC-1 family before branching off independently with their orthologous subunits.

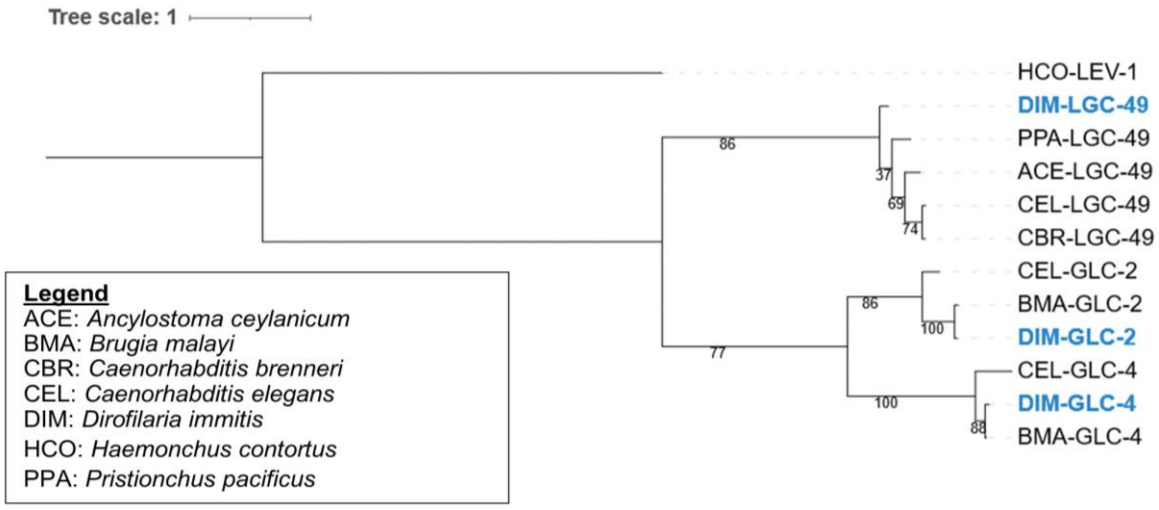

Figure 3.3 – Maximum likelihood phylogenetic tree of Dim-GLC-2, Dim-GLC-4, and Dim-LGC-49 with gene orthologues from other nematode species. The numbers along each branch indicate the bootstrap support percentage values for the subsequent nodes. The tree scale represents changes in evolutionary lineage over time based on the number of amino acid substitutions per site. Refer to the legend for the naming of sequences. Hco-LEV-1, a nicotinic acetylcholine receptor, was used as an outgroup.

3.3 Semi-quantitative end-point PCR

To initially determine the relative expression of Dim-GLC-2, Dim-GLC-4, and Dim-LGC-49, semi-quantitative analysis was done for the adult female, adult male, L3, and Mf life stages. All genes were detected in every life stage of *D. immitis* examined (**Figure 3.4A**). Plotted on the heatmap is the triplicate average gene expression normalized against the positive control (**Figure 3.4B**). The colour of each square is

determined by the number of standard deviations from the mean (Z-score). The relative gene expression is displayed as a gradient from low gene expression (blue) to high gene expression (red) as compared to the average for each gene. For GlC-2, relative expression was highest in adult males followed closely by L3, then adult females, and Mf. GLC-4 was expressed highest in the adult female and Mf, followed by the adult male and L3 life stages. The lowest relatively expressed gene, LGC-49, was expressed consistently in the adult female and Mf life stages, expressed less in adult males, and had the lowest expression in L3 worms. The negative control showed no amplification.

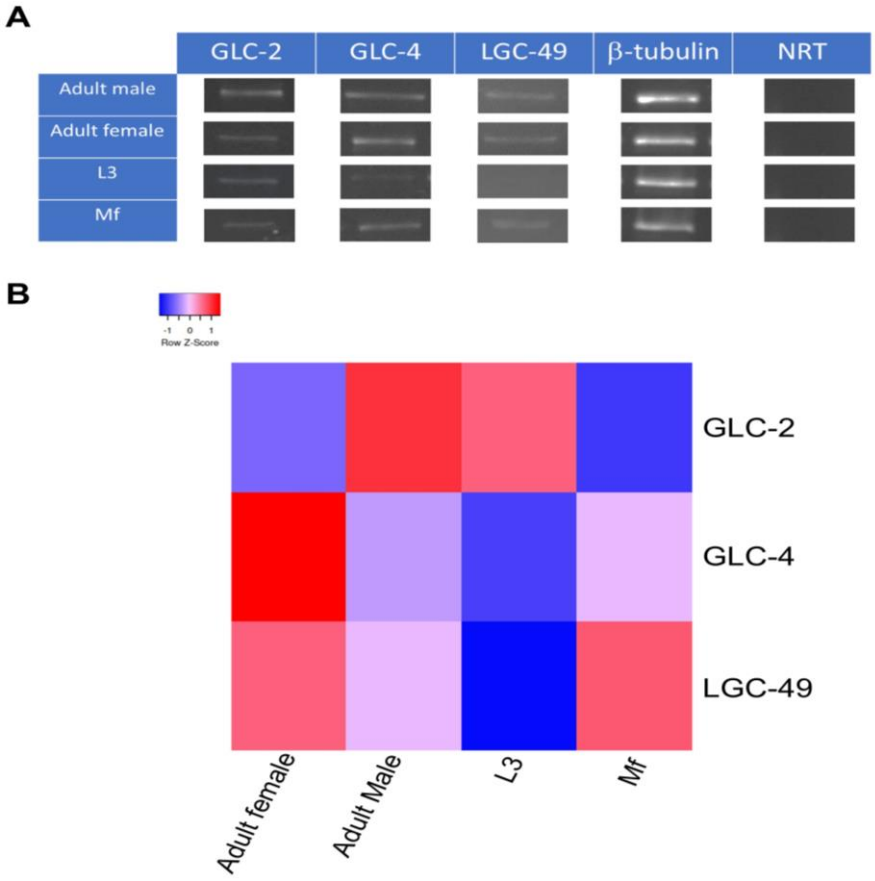

Figure 3.4 – GLC-2, GLC-4 and LGC-49 are expressed in various life stages of *D. immitis*. (**A**) End-point PCR products of cloned *D. immitis* genes. β-tubulin was used as a positive control and NRT reactions were used as a negative control. (**B**) Heatmap displaying the relative gene expression as standard deviations from the mean normalized expression (Z-score) of each gene. The heatmap was made using Heatmapper software (heatmapper.ca).

3.4 RT-qPCR

The RT-qPCR analysis was performed to build upon the semi-quantitative PCR analysis and confirm relative gene expression patterns with a more quantitative approach. For each primer set, standard curves were generated (**A2**). All efficiency values fell within 92.1-109.0%, and linearity correlation values were greater than 0.98 (**A3**), both within the acceptable range according to MIQE guidelines (Bustin *et al.*, 2009) and therefore the qPCR results can be deemed directly comparable. The melt curve analysis gave a single peak for each primer set, indicating high target specificity. The NTC and NRT controls did not show any product amplification.

There was a significant difference between GLC-2 expression in all three life stages examined, with the greatest expression observed in adult males and the lowest in Mf (**Figure 3.5**). The expression of GLC-4 is similar between the adult female and Mf life stages, but it is expressed significantly lower in adult male worms. LGC-49 was also similarly expressed in adult females and Mf, with lowest expression found in adult males. For adult male and female *D. immitis*, LGC-49 was expressed the least when compared to other cloned genes. The gene with the highest expression for the adult female and Mf life stage was GLC-4, and GLC-2 was expressed most in the adult male life stage. For Mf, GLC-2 is the lowest expressed gene of the three studied.

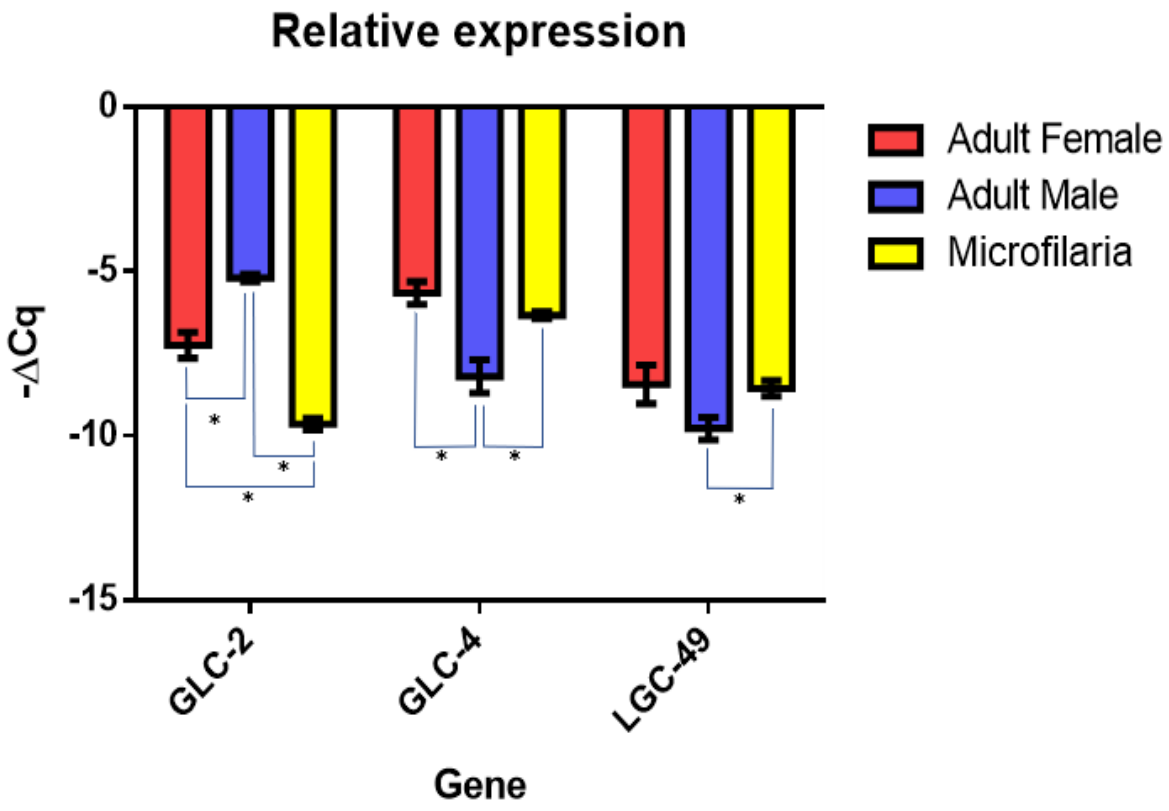

Figure 3.5 – Comparative results of RT-qPCR for the expression of GLC-2, GLC-4, and LGC-49 across *D. immitis* life stages. Relative gene expression was determined by normalizing the Cq values of the gene of interest against two endogenous controls, GAPDH and DITPH. Each bar is the inverse mean normalized Cq values of three biological replicates, each an average of tree technical replicates. (N=3) ± SD.

3.5 Pharmacological characterization of GLC-2, GLC-4, and LGC-49

3.5.1 Dim-GLC-2 and Dim-GLC-4

The *D. immitis* GluCls, GLC-2 and GLC-4, were evaluated for electrophysiological responses alone and co-injected. Oocytes injected with GLC-2 responded consistently to MSG in a dose-dependent manner starting at 500uM (**Figure 3.6A**), whereas the negative control did not respond to MSG at any concentration (**Figure 3.6B**). The MSG EC_{50} value for Dim-GLC-2 was 7.0±1.3mM, and the Hill slope

coefficient was 1.34±0.25, indicating positive cooperativity of agonists (**Figure 3.6C**). All MSG solutions had a pH of approximately 6.

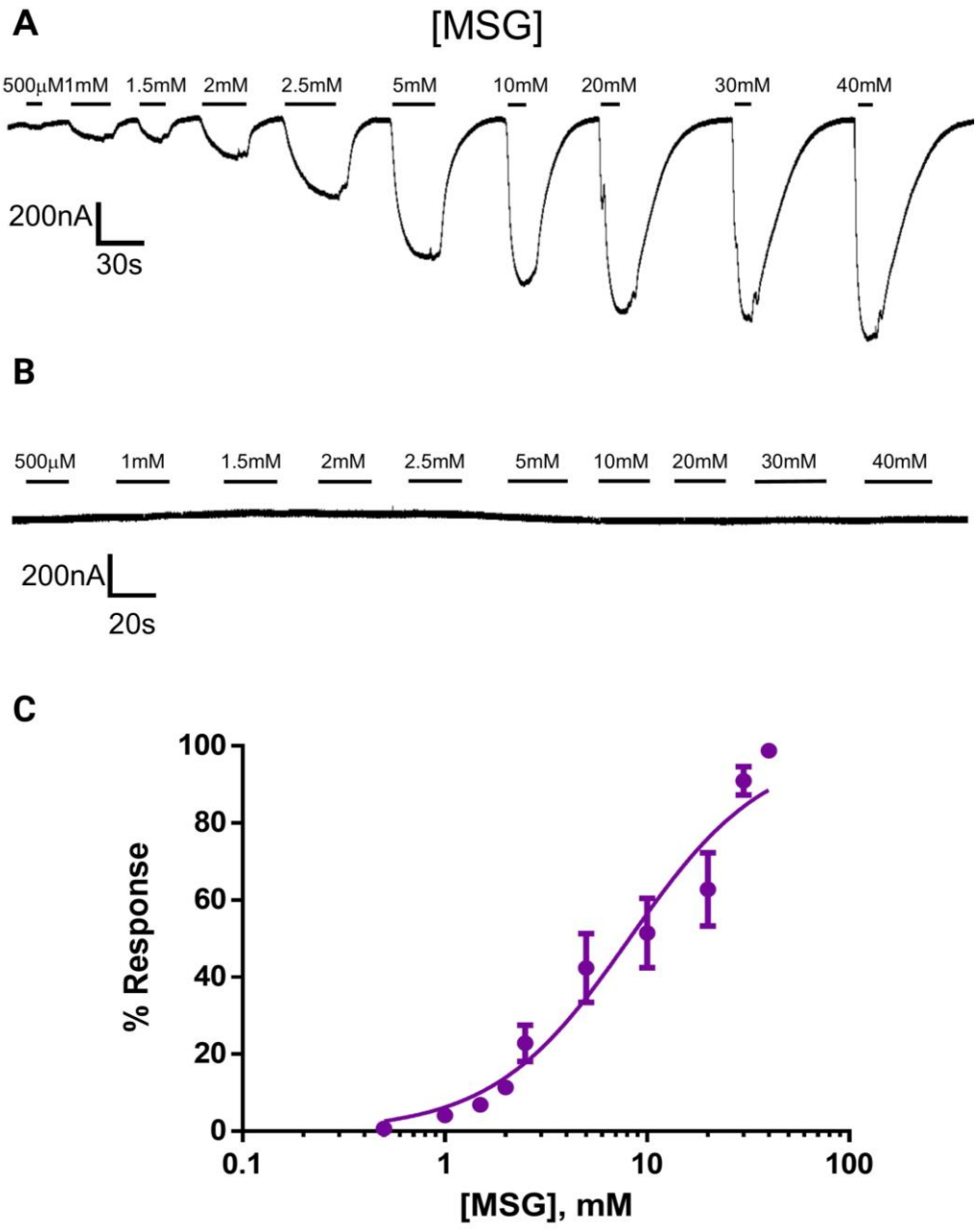

Figure 3.6 – The homomeric Dim-GLC-2 channel is an L-glutamate-gated ion channel. (**A**) Electrophysiological trace of Dim-GLC-2 response to increasing concentrations of MSG. (**B**) Un-injected control oocyte response to the indicated concentrations of MSG. The line below each concentration in both traces indicates how long the molecule was applied. MSG = Monosodium-L-glutamate. nA = nanoamperes. (**C**) Dim-GLC-2 MSG dose-response curve. Standard error shown. N=5, from two batches of frogs.

GLC-2 injected oocytes were also exposed to L-glutamic acid to measure potential responses. The structure of L-glutamic acid and MSG differ as the two carboxylic acid groups of L-glutamic acid are protonated whereas in MSG, the sidechain carboxylic acid is protonated, but the α-carboxylate ion forms an ionic bond with a sodium ion. However, in solution at physiological pH, both of the carboxylic acid groups of L-glutamic acid and MSG are deprotonated, and the structures are identical as the pKa values for the α-carboxylic acid and sidechain carboxylic acid are 2.19 and 4.25, respectively (Hunt, n.d.).

Initial exposure to L-glutamic acid solutions resulted in a depolarization response, whereas MSG produced an expected decrease in current at the same concentration of 5mM (**Figure 3.7A**). The same trend was observed at different ligand concentrations (**Figure 3.7B**). After visualizing the difference in responses caused by the two compounds, the pH of the L-glutamic acid solutions was determined to be approximately 4, which would result in the L-glutamate sidechain carboxylic acid being protonated (Hunt, n.d.). All solutions were adjusted to pH 6 to match the MSG solutions. The pH-adjusted L-glutamic acid solutions elicited larger responses from GLC-2 injected oocytes, but the responses did not follow a discernible dose-dependent pattern in either run for the concentrations tested (**Figure 3.8A**). Based on two replicates, a maximal response appears to occur between concentrations 1.5-2mM. The un-injected control oocytes weakly responded to the L-glutamic acid solutions (**Figure 3.8B**).

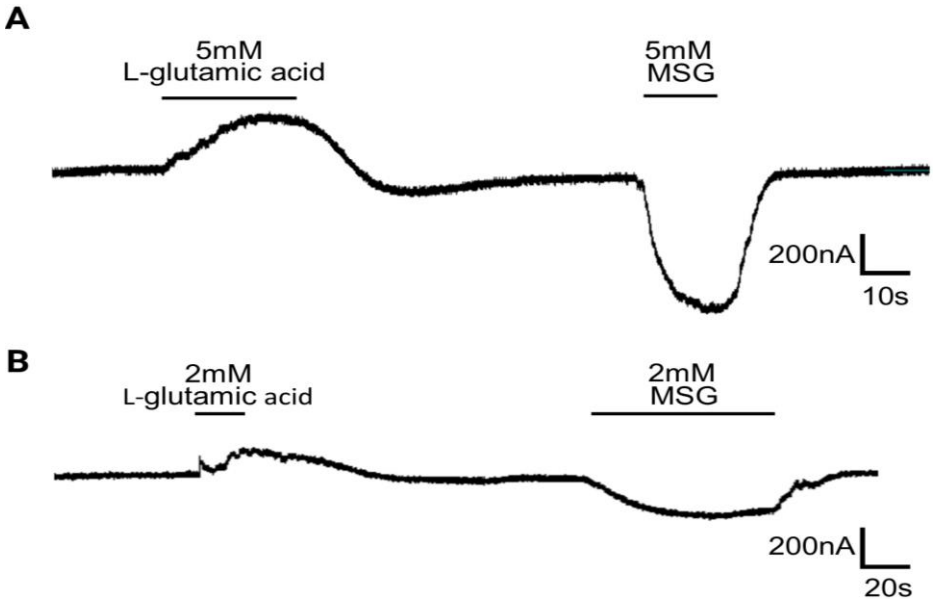

Figure 3.7 – Dim-GLC-2 homomeric channel responds differently to L-glutamic acid and MSG. (**A**) Dim-GLC-2 response to 5mM L-glutamic acid (pH ~4) and 5mM MSG (pH~6). (**B**) Dim-GLC-2 response to 2mM L-glutamic acid (pH ~4) and 2mM MSG (pH~6), demonstrating the same pattern. The line below each concentration indicates how long the molecule was applied. MSG = Monosodium-L-glutamate. nA = nanoamperes.

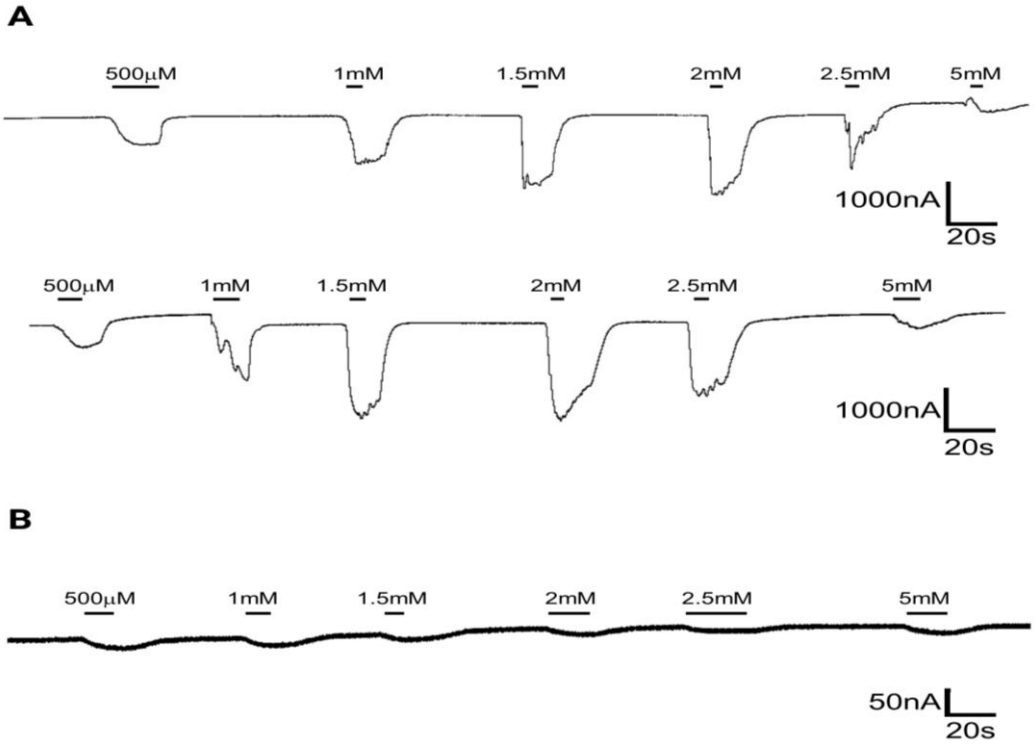

Figure 3.8 – Dim-GLC-2 homomeric channel response to varying concentrations of L-glutamic acid after pH adjustment (pH ~6). The line below each concentration indicates how long the molecule was applied. nA = nanoamperes.

When co-injected with Dim-GLC-2 and Dim-GLC-4, oocyte response to MSG was substantially weaker than when injected with only Dim-GLC-2 but appears to be dose-dependent from the two replicates acquired as no response was seen in the negative control (**Figure 3.9A** and **B**). However, more replicates are required to determine if this response trend exists, as only two were obtained. Oocytes injected with only Dim-GLC-4 did not produce significant currents distinguishable from the un-injected controls when exposed to any solutions tested.

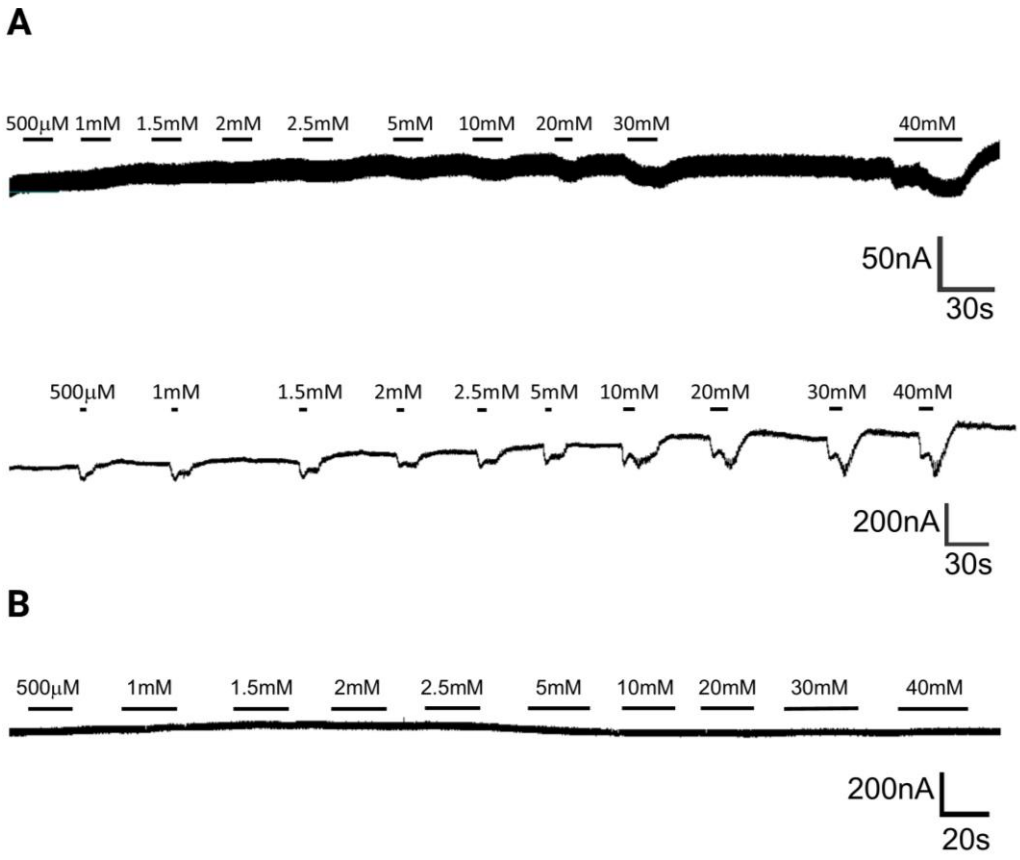

Figure 3.9 – Dim-GLC-2 and Dim-GLC-4 can form functional, albeit less MSG-sensitive, heteromeric channels *in vitro*. (**A**) Dim-GLC-2/Dim-GLC-4 heteromeric channel response to varying concentrations of MSG. (**B**) The negative control oocyte response to the indicated concentrations of MSG. The line below each concentration indicates how long the molecule was applied. nA = nanoamperes.

3.5.2 Dim-LGC-49

Since LGC-49 belongs to the ACC-1 family of cys-loop receptors, acetylcholine was initially tested for a response at 1mM. Acetylcholine generated a significant response from Dim-LGC-49, and a dose-response analysis was conducted (**Figure 3.10A** and **B**). This experiment demonstrated that the LGC-49 response to acetylcholine is dose-dependent, starting at concentrations as low as 25μM and producing a maximum response over 1000nA at 5mM. The acetylcholine EC_{50} value for Dim-LGC-49 was 112μM (n=1) with a Hill slope coefficient of 1.34. More runs are required to confirm this relationship and provide a more accurate EC_{50} value.

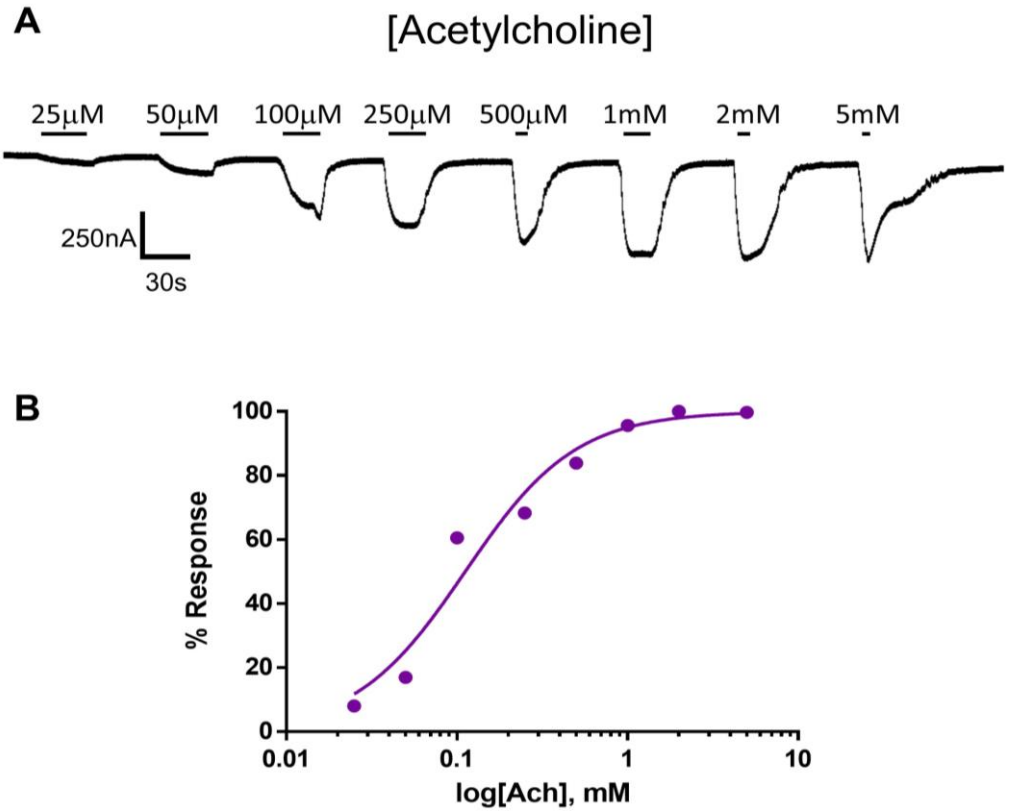

Figure 3.10 – Dim-LGC-49 homomeric channel is an acetylcholine-gated ion channel. (A) Electrophysiological trace Dim-LGC-49 response to increasing concentrations of acetylcholine. The line below each concentration indicates how long the molecule was applied. (**B**) Dim-LGC-49 acetylcholine dose-response curve presented as raw un-normalized response percentage. N=1.

To establish a wider pharmacological profile for LGC-49, other cholinergic compounds were investigated for agonist activity at 1mM based on the initial response to acetylcholine (**Figure 3.11A**). Both levamisole and carbachol elicited a small response from LGC-49 of less than 50nA. Pyrantel produced two paired depolarizing pulses separated by a small inward current followed by a hyperpolarization even after the wash solution was administered. The oocyte did not recover nor return to baseline. More replicates are required to confirm these preliminary responses, as only two were obtained.

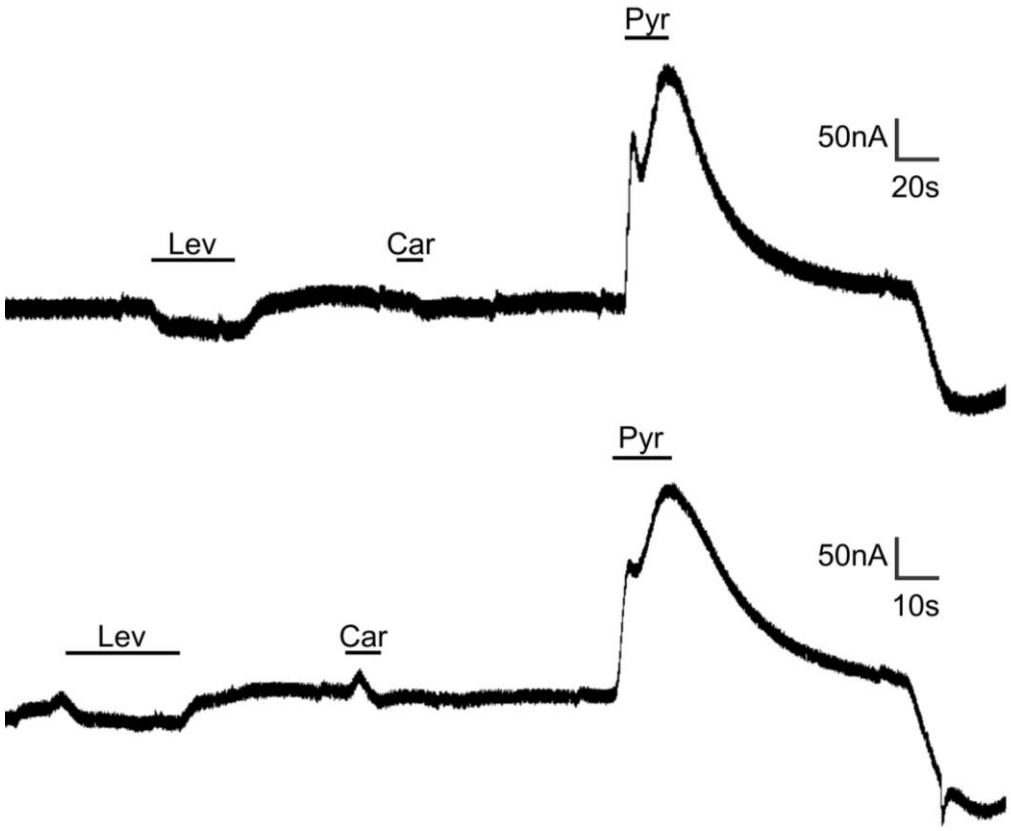

Figure 3.11 – Dim-LGC-49 homomeric channel response to single hits of cholinergic compounds at 1mM. Responses were measured using oocytes from the same frog. The line below each concentration indicates how long the molecule was applied. Lev = levamisole, Car = carbachol, Pyr = pyrantel.

3.6 *In silico* homology protein modelling

3.6.1 Dim-GLC-2

Dim-GLC-2 shares 50.1% sequence identity with the *C. elegans* crystal structure template. The most energetically favourable docking of L-glutamate within the GLC-2 homomeric channel had a binding affinity of -5.7 kcal/mol and had 11 possible residue interactions based on proximity (**Figure 12A**). Ionic hydrogen bonds can form between the polar hydrogens of Ser237 (loop C) and Thr239 (loop C) and the α-carboxylate ion and amine of L-glutamate, respectively. The aromatic residues Phe25, Phe132 (loop A), Tyr192 (loop B), and Tyr244 (loop C) only provide van der Waals interactions as the nitrogen cation of L-glutamate is oriented to the side of the aromatic rings and is too far from the aromatic ring faces to produce cation-π bonds. A repulsive electrostatic interaction potentially occurs between the charged carboxylates of residue Asp27 and the L-glutamate sidechain. Contrarily, the anionic sidechain of L-glutamate has the potential to form attractive electrostatic interactions with the two cationic residues Arg76 (loop G) and Lys214. Residues Pro28 and Ile190 (loop B) offer stabilizing van der Waals interactions.

L-glutamate was also docked within the Dim-GLC-2 homomeric binding pocket to most closely emulate the docking of L-glutamate shown in the Hibbs and Gouaux (2011) published crystal structure of the *C. elegans* GluClα binding site (**Figure 12B** and **C**). The binding affinity for this orientation of L-glutamate was -5.3kcal/mol, and 9 residues were within 4Å of an L-glutamate non-hydrogen atom. Like the more energetically favourable docking model, ionic hydrogen bonds can form with the polar hydrogens of Thr239 and Thr241 (loop C), but these bonds now form with the carboxylate group on

the L-glutamate sidechain. There is potential for two cation-π bonds to form now with the cationic amine group of L-glutamate. The amine is 4.1Å from the aromatic face of residue Tyr192, and while this is close enough to form a cation-π bond, the amine is not positioned at an optimal angle for cation-π bond formation as it is not directly facing the center of the ring. With residue Tyr244, the L-glutamate amine is 3.8Å from the aromatic ring and is positioned at an appropriate angle for a cation-π bond. This is the same residue shown in Hibbs and Gouaux (2011) that forms the essential cation-π bond with L-glutamate. Six residues – Pro28, Asp27, Phe25, Ile190, and Phe132 – offer stabilizing van der Waals interactions with various atoms in L-glutamate. Residues Arg76 and Lys214 are now farther than 4Å from L-glutamate and are not considered part of the binding site.

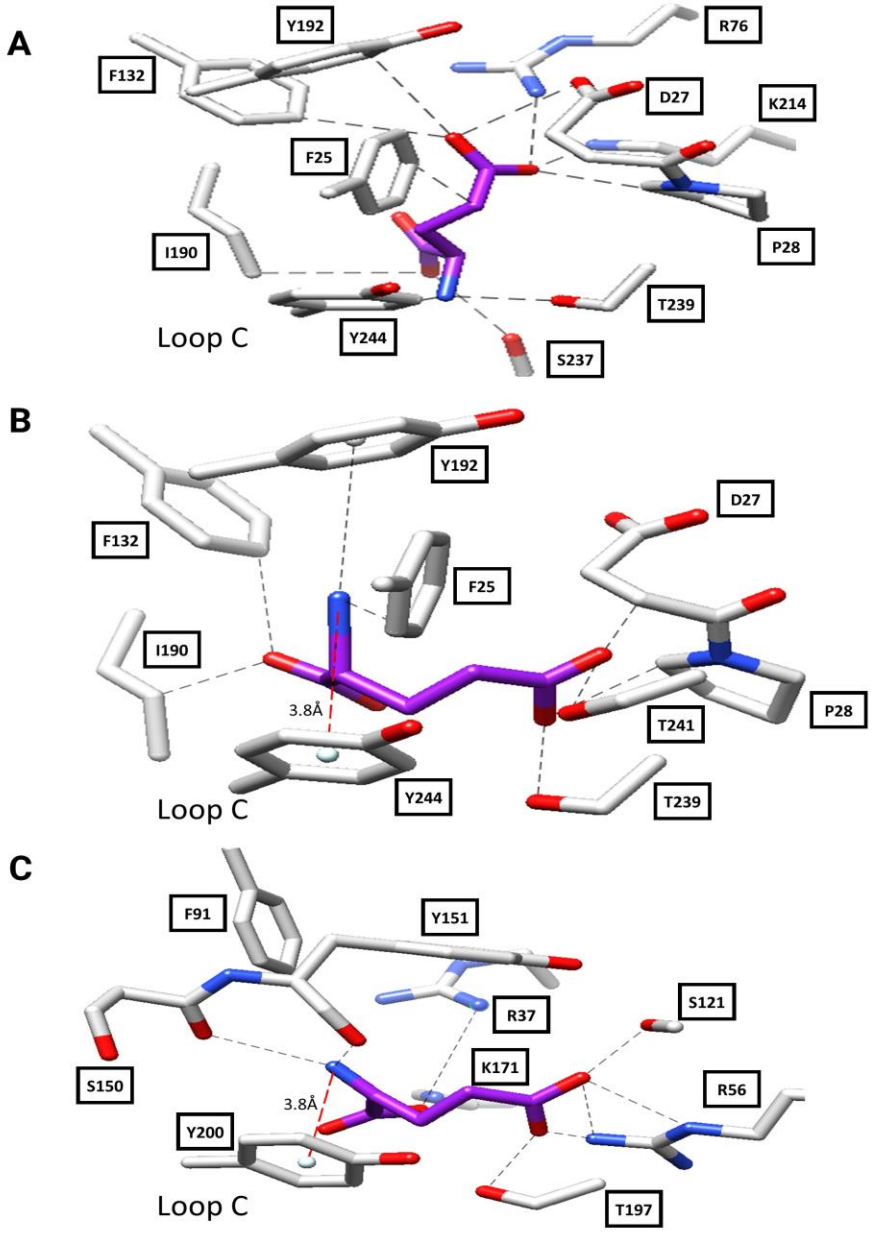

Figure 3.12 – Homology model of Dim-GLC-2 homodimer with L-glutamate docked. (**A**) The most energetically favourable docking of L-glutamate within the Dim-GLC-2 binding pocket. (**B**) The docking of L-glutamate in the Dim-GLC-2 binding pocket which most closely resembles the published crystal structure docking. (**C**) A recreation of the published crystal structure docking of L-glutamate by Hibbs and Gouaux (2011) for comparison. Residues with ligand interactions of 4.0A or less are shown. The distances of potential cation-π bonds are included. Images were captured looking overhead into the binding pocket with binding loop C at the bottom.

3.6.2 Dim-LGC-49

The LGC-49 homomeric channel has 11 residues within 4Å of acetylcholine predicted to contribute to ligand binding (**Figure 3.13**). Dim-LGC-49 shared only a 32.5% sequence identity with the *D. rerio* template, and within the modeled binding pocket, the binding affinity of acetylcholine was -5.1 kcal/mol. The ester oxygen of acetylcholine forms hydrogen bonds with the polar hydrogen of Asn193 (loop E). Similarly, the carbonyl oxygen of acetylcholine's ester hydrogen bonds with Trp271 (loop C). Acetylcholine's quaternary amine can form ionic hydrogen bonds with Asn127 (loop D). Residues Tyr125(loop D), Trp106 (loop G), Tyr266 (loop C), Pro267 (loop C), Ala268 (loop C), Phe222 (loop B), Phe181 (loop E), and Try191 (loop E) all contribute general van der Waal interactions. The cation of acetylcholine is not close enough to the face of any aromatic residues, nor is it directly facing them, to form cation-π bonds.

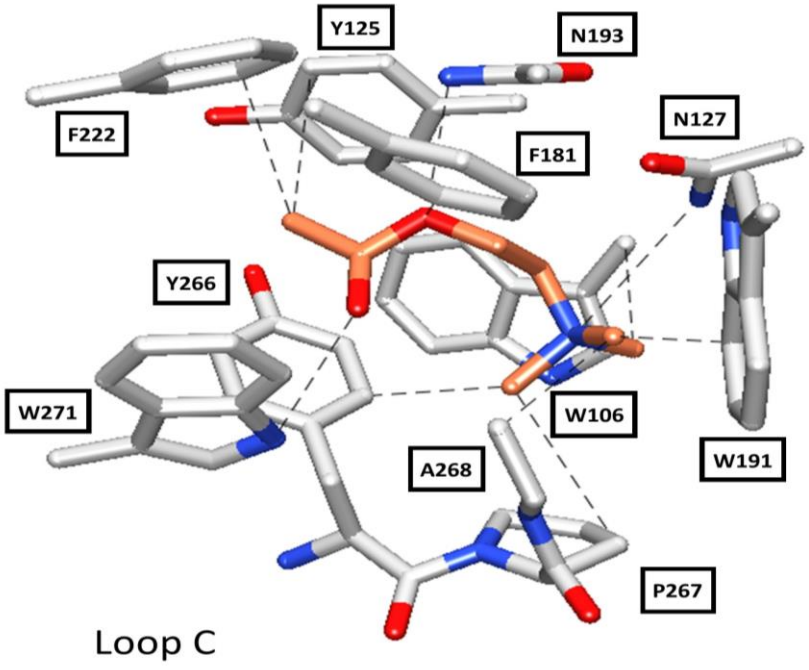

Figure 3.13 - Homology model of Dim-LGC-49 homodimer with acetylcholine docked. Residues with ligand interactions of 4.0A or less are indicated. Images were captured looking overhead into the binding pocket with binding loop C at the bottom.

Chapter 4: Discussion and conclusion

This thesis reports the initial identification and evaluation of novel cys-loop receptor genes from *D. immitis* as potential future drug targets. The subunit genes Dim-GLC-2, Dim-GLC-4, and Dim-LGC-49 are the first members of the AVR-14 and ACC-1 family from this important veterinary parasite to be cloned, characterized, and modelled in the search for more effective anthelminthic targets.

4.1 Characterization of Dim-GLC-2 and Dim-GLC-4

The isolation of the GluCl subunits GLC-2 and GLC-4 described above has shown that these ion channel subunits exist in *D. immitis* and are expressed to varying degrees throughout the parasite's life cycle. Sequencing indicated that both proteins possess the typical features of a cys-loop subunit, and phylogenetic analysis validates that these GluCl subunits are well conserved with other free-living and parasitic nematodes. Electrophysiological evidence provided in this thesis confirms that Dim-GLC-2 can form homomeric channels sensitive to MSG and L-glutamic acid and that Dim-GLC-2 and Dim-GLC-4 can be co-expressed to form a heteromeric channel responsive to MSG. Computational homology modelling highlighted residues which may also play a role in ligand recognition within the GLC-2 binding site of the homomeric channel. This information provides insight into the developmental importance and activation of these channels to be used to improve upon current ML-based anthelmintics or aid in the design of novel drugs which target the GluCls.

Through semi-quantitative analysis and RT-qPCR, it was shown that Dim-GLC-2 is expressed in adult female, adult male, L3, and Mf worms, and that expression significantly differs between the adult female, adult male, and Mf life stages. This subunit

gene is expressed most in adult male and lowest in Mf, which may indicate that while GLC-2 plays a physiological role throughout the life-cycle of *D. immitis*, it may be more involved in the nematode nervous system as the worm matures. Therefore, any novel antiparasitic compound designed to target GLC-2 specifically will likely act strongly against adult worms and offer a new adulticidal alternative to melarsomine hydrochloride.

The relative expression for Dim-GLC-4 differed significantly between the adult male and the adult female and Mf life stages. These findings suggest GLC-4 may be of higher physiological importance to adult females and young larval worms, as opposed to adult males, as expression does not differ significantly between the two life stages. A heartworm treatment that acts against both adult female and Mf worms will stop the infection cycle from propagating as new embryos cannot be produced by the adult females, and the Mf will not survive long enough to procreate. It must also be noted that a drug designed for either GLC-2 or GLC-4 in *D. immitis* is likely to act upon other GluCl subunits within the nematode, like the MLs, due to structural similarities within the same cys-loop family and will elicit a variety of effects across multiple life stages, albeit with different affinities for different subunits.

The relative expression trends from the qPCR analysis did agree with the trends shown in the semi-quantitative PCR analysis for the GluCls, but there are drawbacks to only using the semi-quantitative method to assess gene expression. The results of the semi-quantitative PCRs can be compared between life stages for a single gene, but they cannot be compared between genes for a single life stage as primer efficiencies were not determined. Since the qPCR analysis included averages of the gene expression for three

biological replicates for all life stages, each an average of three technical replicates, and involves a sensitive detection threshold, the qPCR data gives a more accurate representation of relative gene expression in *D. immitis* life stages. Similarly, two controls allow for more reliable normalization (Vandesompele *et al.*, 2002). However, semi-quantitative analysis offers a preliminary determination of relative gene expression to give insight into possible trends between gene expression and life stage without specialized reagents or equipment, providing a less expensive and less time-intensive method to compare the relative expression of genes. The semi-quantitative experiment can be optimized in future analyses to include larger sample sizes, biological replicates, and primers with comparable efficiencies for a more detailed and reliable analysis.

The Dim-GLC-2 homomeric channel was found to be differentially sensitive to MSG and L-glutamic acid despite the structural similarity of the two compounds. In theory, the GLC-2 homomeric channel response to MSG and L-glutamic acid should be similar if not the same, but in reality, it showed much higher affinity to L-glutamic acid once pH adjusted. Sodium bicarbonate, used in the pH adjustment, increases sodium concentration in the perfusion solution, which increases extracellular Na+ concentration and causes inward currents through endogenous *X. laevis* oocyte channels (Xu *et al.*, 2020). This explains the small control responses to the pH-adjusted L-glutamic acid solutions and perhaps why the responses were so much larger than those caused by MSG in GLC-2 injected oocytes. Un-injected oocytes showed no response to MSG, so it is unlikely that the slight increase in sodium concentration from MSG dissociation impacted endogenously expressed *X. laevis* channels. Still, the exact cause of this difference in response remains unknown, but this thesis reports the first instance of nematode GluCl

channel activation by MSG. In rats, MSG has proven effective at decreasing the fecundity and survivability of tapeworms with a single dose of 1g (Webb, 1995). While MSG has yet to be tested on whole nematodes or in infected canines, the administration of MSG may be a beneficial addition to current heartworm treatments in small quantities.

Dose-response analysis for Dim-GLC-2 determined a high EC_{50} value for MSG of 7.0mM. For experiments with L-glutamic acid, responses were observed starting at 500μM and appeared to reach a maximum at approximately 2mM. Therefore, the estimated EC_{50} value for L-glutamic acid is estimated to be over 500μM and below 2mM, and shows that GLC-2 has a lower sensitivity to L-glutamic acid than MSG. However, further study is required to determine the differences between MSG and L-glutamic acid on channel activation. In *C. elegans*, the reported GLC-2 homomeric channel EC_{50} value for L-glutamate was 214μM (Lamassiaude *et al.*, 2022). The findings of this thesis suggest that the Dim-GLC-2 channel is less sensitive to L-glutamate in the tested forms compared to the Cel-GLC-2 channel.

The electrophysiology results for oocytes injected with Dim-GLC-4 concurs with that of published literature for oocytes injected with Cel-GLC-4 (Pelligrino, 2022) or Bma-GLC-4 (Lamassiaude *et al.*, 2022) as they failed to respond to L-glutamate. GLC-4 may not be able to express as homomeric channels in *X. laevis* oocytes, and either needs to be co-expressed with other GluCl subunits to form a heteromeric channel or co-injected with accessory proteins to form a functional homomeric channel. It may also be that homomeric channels form in this heterologous expression system but that they have a much lower affinity than other GluCl subunits for the tested ligands.

Small currents were observed when GLC-2 was co-expressed with GLC-4. It is possible that the two subunits form a heteromeric channel with a decrease in channel sensitivity to L-glutamate in the form of MSG. In *C. elegans*, the co-expression of Cel-GLC-2 and Cel-GLC-4 resulted in a 15-fold decrease in glutamate sensitivity compared to Cel-GLC-2 alone (Lamassiaude *et al.*, 2022). A similar pattern can be observed with *D. immitis* in the evidence provided in this thesis. The MSG responses in oocytes expressing only GLC-2 were substantially greater than those of the oocytes expressing both GLC-2 and GLC-4. Therefore, it is likely that the GLC-4 subunit suppresses glutamate sensitivity, but the fold decrease will need to be determined pending more data for the heteromeric channel. Additionally, in *B. malayi*, the solo-injection and co-injection of Bma-GLC-2 and Bma-GLC-4 did not result in the formation of glutamate-responsive channels (Lamassiaude *et al.*, 2022). It is interesting that the response pattern for *D. immitis* GluCl channels more closely follows that of a free-living nematode from clade V rather than that of a closely related, parasitic nematode from the same clade.

Homology models were produced only for homomeric receptors that showed activation from tested agonists. The Dim-GLC-2 homomeric channel binding pocket highlighted important residues that can be exploited in the design of novel antiparasitics with higher receptor binding affinity. Within the most energetically favourable model, the strongest interactions within 4Å of L-glutamate were the attractive electrostatic interactions with residues Arg76 and Lys214 and the repulsive electrostatic interactions with Asp27. In contrast, the strongest bond from the GLC-2 docking model which most closely resembled that of Hibbs and Gouaux (2011) was a 3.8Å cation-π bond with residue Tyr244 – the same length of the cation-π bond between L-glutamate and Tyr200

of the published crystal structure. Between the GLC-2 docking models, the second saw the loss of these three electrostatic interactions and an ionic hydrogen bond with Ser237 but did gain an ionic hydrogen bond with residue Thr241. To explain the difference in binding affinity, the existence of the three electrostatic interactions may result in a more favourable docking of L-glutamate within the binding pocket than a single π-cation interaction.

4.2 Characterization of Dim-LGC-49

LGC-49 is the first subunit from the ACC-1 family to be cloned and characterized from *D. immitis*. Sequencing and phylogenetic analysis results indicated that the Dim-LGC-49 protein contains the usual features of a cys-loop subunit and the PAR motif present in other anion-selective channels and that the sequence is well-conserved across nematode species and clades. Both semi-quantitative and RT-qPCR results showed LGC-49 is expressed throughout the life of *D. immitis*, signifying its persistent physiological relevance in the parasite. Dim-LGC-49 can form functional homomeric channels responsive to acetylcholine and other cholinergic compounds, as is evident by the electrophysiological results. The homology model of LGC-49 with acetylcholine docked identified residues potentially responsible for cholinergic ligand recognition. Overall, the information obtained from this thesis can contribute to the design of heartworm medications that target LGC-49 and the whole family of ACC-1 receptors.

Of the three genes examined in this thesis, LGC-49 showed the least significant variation between the adult female, adult male, and Mf life stages. Expression trends provided by the semi-quantitative analysis match that of the RT-qPCR analysis. The LGC-49 expression only differs significantly between adult males and Mf worms.

Therefore, a drug designed to activate this specific channel may exert effects spanning multiple life stages. However, LGC-49 was also the gene with the lowest overall normalized expression compared to the GluCls reviewed. So, while an LGC-49-specific anthelmintic may impact multiple life stages of *D. immitis*, it may not elicit the strongest physiological response from the worm. Despite this, the novel drug will likely also target other members of the ACC-1 LGIC subgroup due to sequence similarity, possibly eliciting a strong nematocidal effect.

Electrophysiological analysis confirmed that the Dim-LGC-49 homomeric channel is responsive to acetylcholine at low μM concentrations and weakly responsive to the cholinomimetic drugs carbachol, levamisole, and pyrantel at 1mM concentrations. The data for the dose-response analysis of LGC-49 and acetylcholine was presented based on a single run due to difficulties with repeated ligand applications, a problem also encountered by Hardege *et al.* (2023) when working with Cel-LGC-49. However, Hardege *et al.* (2023) still determined the Cel-LGC-49 EC_{50} value for acetylcholine was 19μM. Compared to the Dim-LGC-49 EC_{50} value for acetylcholine of 112μM, this shows the *D. immitis* homomeric channel has an almost 5-fold decreased sensitivity to the natural ligand. Additionally, the LGC-49 outward response to pyrantel appears to be abnormal as other ACC-1 subunits characterized from the parasitic nematode *H. contortus* show an inward current when pyrantel is applied (Habibi *et al.*, 2018; Habibi *et al.*, 2020). The observed response pattern is synonymous with the electrophysiological traces of follicle-enclosed *X. laevis* oocytes in responses to acetylcholine or, oddly enough, more closely to that of follicle-stimulating hormone (Arellano and Miledi, 1993). The typical response includes three phases: 1) a large outward current, 2) a short but

small inward current, and 3) a slow but long-lasting outward current linked to a decrease in membrane ion conductance – all seen in the LGC-49 pyrantel response. The cause of this unusual response to pyrantel in *lgc-49*-injected oocytes will require additional research.

The docking of acetylcholine within the Dim-LGC-49 binding pocket revealed 11 residues that potentially interact with the ligand, the strongest being the ionic hydrogen bond with Asn127 of loop D. Homology modelling for other ACC-1 subunits from *H. contortus*, including ACC-2, LGC-46, and the heteromeric channel ACC-1/ACC-2, all emphasized three residues within the binding pocket that were essential for agonist recognition: a phenylalanine residue in loop B, a tryptophan residue in loop C, and a asparagine residue in loop E (Callanan *et al.*, 2018; Habibi *et al.*, 2018; Habibi *et al.*, 2020). The residues Trp271 of loop C, Phe222 of loop B, and Asn193 of loop E for Dim-LGC-49 coincide with these important residues. However, the most energetically favourable position of acetylcholine within the binding pocket does not allow for any interaction other than van der Waals to exist with the two aromatic residues Trp271 and Phe222 due to its distance from the centre of the rings. In the other ACC-1 subgroup models, acetylcholine orientation is flipped, with the quaternary amine of acetylcholine fitting between the two aromatic residues and the carbonyl oxygen of acetylcholine's ester hydrogen bonding with the asparagine residue. Since this is a hypothetical model, the actual docking of acetylcholine may more closely resemble that of the computational homology models of other ACC-1 receptors, but additional experiments are needed.

4.3 Future work

Performing additional RT-qPCR experiments can add to the current knowledge of receptor expression throughout the lifetime of *D. immitis* and highlight which life stages may be the most susceptible to novel anthelmintics. Relative expression should be measured for other AVR-14 and ACC-1 subunits to get a more comprehensive look at which receptors have a higher expression and, consequently, a greater physiologic importance, in the nematode. To supplement this, subunit immunolocalization experiments performed on different life stages of *D. immitis* will show how each receptor subunit is differentially expressed at various points in worm development and in which tissues they are predominant. Overlaying the expression patterns of different subunits can also provide additional information, such as if subunits are co-localized and, potentially, if they form heteromeric channels *in vivo*.

Based on the characterization of orthologous subunits, it is assumed that GLC-2, GLC-4, and LGC-49 form anionic-selective channels. While this is most likely the case, it has not yet been proven for these subunits in *D. immitis*. Therefore, a current-voltage analysis performed with TEVC electrophysiology should be done to confirm that these channels are selective for chloride ions.

This study offered an initial pharmacological characterization of three cys-loops subunits with potential to be the targets of novel anthelmintics. It should be noted that the EC_{50} values produced in *Xenopus* oocytes do not always match the endogenous *in vivo* EC_{50} of these channels, but this heterologous expression system provides an excellent starting point in receptor characterization despite the occasional drawback. Factors such as diminished *X. laevis* egg quality limited the data able to be collected for several

electrophysiology experiments in this thesis. Wild *X. laevis* females can produce good-quality eggs even past prime reproductive age (4.5-15 years old), but this is not the same for commercially bred frogs (Green, 2002). Therefore, it would be beneficial to perform replicates of the electrophysiology experiments performed for this thesis on oocytes from younger frogs to add to the initial results and provide a more accurate view of ligand activation. In addition, other electrophysiology experiments can build upon the current pharmacological profiles of the cloned *D. immitis* cys-loop subunits. This may include the administration of current anthelmintics to measure channel sensitivity, testing the pH-adjusted L-glutamic acid solutions at concentrations lower than 500μM to see if responses are dose-dependent, and testing traditional antagonists to determine their influence on channel activation. Receptor subunits should also be co-injected with other subunits from their cys-loop LGIC subgroups to see if functional heteromeric channels can form.

Finally, homology modelling visualizes potentially important residues responsible for agonist recognition, but all modelling and docking presented in this thesis are hypothetical and require experimental verification. Site-directed mutagenesis can confirm the importance of specific residues by introducing a point-mutation within the gene sequence to produce an altered protein. Normally a single residue is changed into an alanine so it loses all functionality. In the case of GLC-2, the Tyr244 residue may be involved with a cation-π bond formation in the binding site with L-glutamate, but this is not the most energetically favourable ligand position according to the affinity values of generated models despite being highlighted in the published crystal structure of the template. Similarly, for LGC-49, the residues Trp271, Phe222, and Asn193 are all

predicted to offer relatively weak bonds, whereas the corresponding residues in other models of ACC-1 subgroup channels offer stronger interactions in comparison. The mutation of any of these residues will corroborate their importance within the binding pocket based on additional TEVC electrophysiology experiments with the mutants.

4.4 Conclusion

This thesis provides the first steps of the target-based drug discovery process and adds to the current knowledge of the AVR-14 and ACC-1 families of cys-loop LGIC subunits as potential drug targets for heartworm treatments. Phylogenetic analysis shows these genes are conserved across the phyla, and if a novel drug targeted these receptors, it would have a broad spectrum of action. The semi-quantitative and RT-qPCR results show that each gene is expressed in the adult female, adult male, L3, and Mf life stages to varying degrees. The electrophysiology experiments conducted show LGC-49 and GLC-2 can form functional homomeric channels, and GLC-2 and GLC-4 produce MSG-sensitive heteromeric channels in *Xenopus* oocytes. Both *D. immitis* LGC-49 and GLC-2 homomeric channels show decreased sensitivity to their natural ligands compared to those of *C. elegans*. LGC-49 is responsive to acetylcholine at lower concentrations than either GluCl as homomeric or heteromeric channels to L-glutamate in its different forms. Currently there are no drugs that target the ACC-1 gene family. This subgroup of receptors are attractive targets as they are invertebrate-specific and expressed in different developmental stages of *D. immitis*. However, all subunits presented in this thesis may be suitable drug targets for antiparasitic drugs but require further characterization and evaluation to realize their true capacity for anthelmintic action.

In conclusion, the AVR-14 subunits, GLC-2 and GLC-4, and the ACC-1 subunit, LGC-49, highlight three proteins that are well-suited to be studied further in the search for new targets for rational drug screening. Future drug designs that target the cys-loop receptors identified by this research may prove more effective and cause fewer harmful side effects than present methods. With the rapid and drastic increase in drug-resistant strains of parasitic nematodes, it is essential that the properties of *D. immitis* cys-loop LGICs be evaluated to aid in the development of improved heartworm treatments and to benefit veterinary practices worldwide.

BIBLIOGRAPHY

American Academy of Veterinary Pharmacology & Therapeutics. (2008). Melarsomine veterinary—systemic. American Academy of Veterinary Pharmacology & Therapeutics. https://cdn.ymaws.com/www.aavpt.org/resource/resmgr/imported/melarsomine.pdf

Antiabong, J. F., Ngoepe, M. G., & Abechi, A. S. (2016). Semi-quantitative digital analysis of polymerase chain reaction-electrophoresis gel: Potential applications in low-income veterinary laboratories. *Veterinary World*, *9*(9), 935–939. https://doi.org/10.14202/vetworld.2016.935-939

Anvari, D., Narouei, E., Daryani, A., Sarvi, S., Moosazadeh, M., Ziaei Hezarjaribi, H., Narouei, M. R., & Gholami, S. (2020). The global status of Dirofilaria immitis in dogs: A systematic review and meta-analysis based on published articles. *Research in Veterinary Science*, *131*, 104–116. https://doi.org/10.1016/j.rvsc.2020.04.002

Arellano, R., & Miledi, R. (1993). Novel Cl- currents elicited by follicle stimulating hormone and acetylcholine in follicle-enclosed Xenopus oocytes. *The Journal of General Physiology*, *102*(5), 833–857. https://doi.org/10.1085/jgp.102.5.833

Bowman, D. D. (2012). Heartworms, macrocyclic lactones, and the specter of resistance to prevention in the United States. *Parasites & Vectors*, *5*, Article 138. https://doi.org/10.1186/1756-3305-5-138

Bowman, D. D., & Drake, J. (2017). Examination of the "susceptibility gap" in the treatment of canine heartworm infection. *Parasites & Vectors*, *10*(Suppl 2), 513. https://doi.org/10.1186/s13071-017-2433-9

Bustin, S. A., Benes, V., Garson, J. A., Hellemans, J., Huggett, J., Kubista, M., Mueller, R., Nolan, T., Pfaffl, M. W., Shipley, G. L., Vandesompele, J., & Wittwer, C. T. (2009). The MIQE Guidelines: Minimum Information for Publication of Quantitative Real-Time PCR Experiments. *Clinical Chemistry*, *55*(4), 611–622. https://doi.org/10.1373/clinchem.2008.112797

Callanan, M. K., Habibi, S. A., Law, W. J., Nazareth, K., Komuniecki, R. L., & Forrester, S. G. (2018). Investigating the function and possible biological role of an acetylcholine-gated chloride channel subunit (ACC-1) from the parasitic nematode Haemonchus contortus. *International Journal for Parasitology. Drugs and Drug Resistance*, *8*(3), 526–533. https://doi.org/10.1016/j.ijpddr.2018.10.010

Chen, K., & Kurgan, L. (2009). Investigation of Atomic Level Patterns in Protein—Small Ligand Interactions. *PLoS ONE*, *4*(2), e4473. https://doi.org/10.1371/journal.pone.0004473

Choudhary, S., Kashyap, S. S., Martin, R. J., & Robertson, A. P. (2022). Advances in our understanding of nematode ion channels as potential anthelmintic targets.

International Journal for Parasitology: Drugs and Drug Resistance, *18*, 52–86. https://doi.org/10.1016/j.ijpddr.2021.12.001

Coghlan, A., Tyagi, R., Cotton, J. A., Holroyd, N., Rosa, B. A., Tsai, I. J., Laetsch, D. R., Beech, R. N., Day, T. A., Hallsworth-Pepin, K., Ke, H.-M., Kuo, T.-H., Lee, T. J., Martin, J., Maizels, R. M., Mutowo, P., Ozersky, P., Parkinson, J., Reid, A. J., … International Helminth Genomes Consortium. (2019). Comparative genomics of the major parasitic worms. *Nature Genetics*, *51*(1), Article 1. https://doi.org/10.1038/s41588-018-0262-1

Geary, T. G., Bourguinat, C., & Prichard, R. K. (2011). Evidence for Macrocyclic Lactone Anthelmintic Resistance in Dirofilaria immitis. *Topics in Companion Animal Medicine*, *26*(4), 186–192. https://doi.org/10.1053/j.tcam.2011.09.004

Green, S. L. (2002). Factors Affecting Oogenesis in the South African Clawed Frog (Xenopus laevis). *Comparative Medicine*, *52*(4). PMID: 12211272

Habibi, S. A., Callanan, M., & Forrester, S. G. (2018). Molecular and pharmacological characterization of an acetylcholine-gated chloride channel (ACC-2) from the parasitic nematode Haemonchus contortus. *International Journal for Parasitology: Drugs and Drug Resistance*, *8*(3), 518–525. https://doi.org/10.1016/j.ijpddr.2018.09.004

Habibi, S. A., Blazie, S. M., Jin, Y., & Forrester, S. G. (2020). Isolation and characterization of a novel member of the ACC ligand-gated chloride channel family, Hco-LCG-46, from the parasitic nematode Haemonchus contortus. *Molecular and Biochemical Parasitology*, *237*, 111276. https://doi.org/10.1016/j.molbiopara.2020.111276

Hardege, I., Morud, J., Courtney, A., & Schafer, W. R. (2023). A Novel and Functionally Diverse Class of Acetylcholine-Gated Ion Channels. *The Journal of Neuroscience*, *43*(7), 1111–1124. https://doi.org/10.1523/JNEUROSCI.1516-22.2022

Hibbs, R. E., & Gouaux, E. (2011). Principles of activation and permeation in an anion-selective Cys-loop receptor. *Nature*, *474*(7349), Article 7349. https://doi.org/10.1038/nature10139

Hunt, I. (n.d.). *Ch27 pKa and pI values.* Chapter 27: Amino Acids, Peptides and Proteins. UCalgary. https://www.chem.ucalgary.ca/courses/351/Carey5th/Ch27/ch27-1-4-2.html

Infield, D. T., Rasouli, A., Galles, G. D., Chipot, C., Tajkhorshid, E., & Ahern, C. A. (2021). Cation-π interactions and their functional roles in membrane proteins. *Journal of Molecular Biology*, *433*(17), 167035. https://doi.org/10.1016/j.jmb.2021.167035

Jacobson, L. S., Ward, K. A., Lacaden, A. B., & Hornak, T. A. (2020). Prevalence of heartworm in relocated, local and outreach clinic dogs: A Canadian sheltering perspective. *Veterinary Parasitology*, *283*, 109081. https://doi.org/10.1016/j.vetpar.2020.109081

Jensen, M. L., Timmermann, D. B., Johansen, T. H., Schousboe, A., Varming, T., & Ahring, P. K. (2002). The beta subunit determines the ion selectivity of the GABAA receptor. *The Journal of Biological Chemistry*, *277*(44), 41438–41447. https://doi.org/10.1074/jbc.M205645200

Jones, A. K., & Sattelle, D. B. (2008). The cys-loop ligand-gated ion channel gene superfamily of the nematode, Caenorhabditis elegans. *Invertebrate Neuroscience*, *8*(1), 41–47. https://doi.org/10.1007/s10158-008-0068-4

Knight, D. H., & Lok, J. B. (1998). Seasonality of heartworm infection and implications for chemoprophylaxis. *Clinical Techniques in Small Animal Practice*, *13*(2), 77–82. https://doi.org/10.1016/S1096-2867(98)80010-8

Kumar, A., Basak, S., Rao, S., Gicheru, Y., Mayer, M. L., Sansom, M. S. P., & Chakrapani, S. (2020). Mechanisms of activation and desensitization of full-length glycine receptor in lipid nanodiscs. *Nature Communications*, *11*(1), Article 1. https://doi.org/10.1038/s41467-020-17364-5

Laing, R., Kikuchi, T., Martinelli, A., Tsai, I. J., Beech, R. N., Redman, E., Holroyd, N., Bartley, D. J., Beasley, H., Britton, C., Curran, D., Devaney, E., Gilabert, A., Hunt, M., Jackson, F., Johnston, S. L., Kryukov, I., Li, K., Morrison, A. A., … Cotton, J. A. (2013). The genome and transcriptome of Haemonchus contortus, a key model parasite for drug and vaccine discovery. *Genome Biology*, *14*(8), article 8. https://doi.org/10.1186/gb-2013-14-8-r88

Lamassiaude, N., Courtot, E., Corset, A., Charvet, C. L., & Neveu, C. (2022). Pharmacological characterization of novel heteromeric GluCl subtypes from Caenorhabditis elegans and parasitic nematodes. *British Journal of Pharmacology*, *179*(6), 1264–1279. https://doi.org/10.1111/bph.15703

Li, J., Zhang, Z., Xu, C., Wang, D., Lv, M., & Xie, H. (2020). Identification and validation of reference genes for real-time RT-PCR in Aphelenchoides besseyi. *Molecular Biology Reports*, *47*(6), 4485–4494. https://doi.org/10.1007/s11033-020-05547-8

McGill, E., Berke, O., Peregrine, A. S., & Weese, J. S. (2019a). Epidemiology of canine heartworm (Dirofilaria immitis) infection in domestic dogs in Ontario, Canada: Geographic distribution, risk factors and effects of climate. *Geospatial Health*, *14*(1), Article 1. https://doi.org/10.4081/gh.2019.741

McGill, E., Berke, O., Weese, J. S., & Peregrine, A. (2019b). Heartworm infection in domestic dogs in Canada, 1977–2016: Prevalence, time trend, and efficacy of

prophylaxis. *The Canadian Veterinary Journal*, *60*(6), 605–612. PMCID: PMC6515813; PMID: 31156260

Meot-Ner (Mautner), M. (2005). The Ionic Hydrogen Bond. *Chemical Reviews*, *105*(1), 213–284. https://doi.org/10.1021/cr9411785

Morris, G. M., Huey, R., Lindstrom, W., Sanner, M. F., Belew, R. K., Goodsell, D. S., & Olson, A. J. (2009). AutoDock4 and AutoDockTools4: Automated docking with selective receptor flexibility. *Journal of Computational Chemistry*, *30*(16), 2785–2791. https://doi.org/10.1002/jcc.21256

Noack, S., Harrington, J., Carithers, D. S., Kaminsky, R., & Selzer, P. M. (2021). Heartworm disease – Overview, intervention, and industry perspective. *International Journal for Parasitology: Drugs and Drug Resistance*, *16*, 65–89. https://doi.org/10.1016/j.ijpddr.2021.03.004

Pellegrino, M. (2002). Association between GLC-4 and AVR-14: Role of GluCl subunit composition in Caenorhabditis elegans ivermectin sensitivity and behaviour. (Master's thesis). McGill University. https://escholarship.mcgill.ca/concern/theses/h415pb046

Pettersen. (2004). UCSF Chimera—A visualization system for exploratory research and analysis. *Journal of Computational Chemistry*. https://onlinelibrary-wiley-com.uproxy.library.dc-uoit.ca/doi/full/10.1002/jcc.20084

Putrenko, I., Zakikhani, M., & Dent, J. A. (2005). A Family of Acetylcholine-gated Chloride Channel Subunits in Caenorhabditis elegans*. *Journal of Biological Chemistry*, *280*(8), 6392–6398. https://doi.org/10.1074/jbc.M412644200

Reddy, M. V. (2013). Human dirofilariasis: An emerging zoonosis. *Tropical Parasitology*, *3*(1), 2–3. PMCID: PMC3745666; PMID: 23961434

Simón, F., Siles-Lucas, M., Morchón, R., González-Miguel, J., Mellado, I., Carretón, E., & Montoya-Alonso, J. A. (2012). Human and Animal Dirofilariasis: The Emergence of a Zoonotic Mosaic. *Clinical Microbiology Reviews*, *25*(3), 507–544. https://doi.org/10.1128/cmr.00012-12

Sneed, S. D., Dwivedi, S. B., DiGate, C., Denecke, S., & Povelones, M. (2022). Aedes aegypti Malpighian tubules are immunologically activated following systemic Toll activation. *Parasites & Vectors*, *15*, 469. https://doi.org/10.1186/s13071-022-05567-2

Thompson, A. J., Lester, H. A., & Lummis, S. C. R. (2010). The structural basis of function in Cys-loop receptors. *Quarterly Reviews of Biophysics*, *43*(4), 449–499. https://doi.org/10.1017/S0033583510000168

Thompson, S. J. (2016). *Determination of a Gene Expressed only in the Infective Larval Stage of Dirofilaria immitis* (Master's thesis). Valdosta State University. http://hdl.handle.net/10428/2175

Trott, O. & Olson., A. J. (2009). AutoDock Vina: Improving the speed and accuracy of docking with a new scoring function, efficient optimization, and multithreading. *Journal of Computational Chemistry*. https://doi-org.uproxy.library.dc-uoit.ca/10.1002/jcc.21334

Vandesompele, J., De Preter, K., Pattyn, F., Poppe, B., Van Roy, N., De Paepe, A., & Speleman, F. (2002). Accurate normalization of real-time quantitative RT-PCR data by geometric averaging of multiple internal control genes. *Genome Biology*, *3*(7), RESEARCH0034. https://doi.org/10.1186/gb-2002-3-7-research0034

Webb, R. A. (1995). An acute dose of monosodium-l-glutamate causes decreased fecundity and enhanced loss of the cestode Hymenolepis diminuta from rats. *Parasitology Research*, *81*(3), 202–206. https://doi.org/10.1007/BF00937110

Weston, D., Patel, B., & Van Voorhis, W. C. (1999). Virulence in Trypanosoma cruzi infection correlates with the expression of a distinct family of sialidase superfamily genes. *Molecular and Biochemical Parasitology*, *98*(1), 105–116. https://doi.org/10.1016/S0166-6851(98)00152-2

Williamson, S. M., Walsh, T. K., & Wolstenholme, A. J. (2007). The cys-loop ligand-gated ion channel gene family of Brugia malayi and Trichinella spiralis: A comparison with Caenorhabditis elegans. *Invertebrate Neuroscience*, *7*(4), 219–226. https://doi.org/10.1007/s10158-007-0056-0

Wolstenholme, A. J. (2011). Ion channels and receptor as targets for the control of parasitic nematodes. *International Journal for Parasitology: Drugs and Drug Resistance*, *1*(1), 2–13. https://doi.org/10.1016/j.ijpddr.2011.09.003

Wolstenholme, A. J., Evans, C. C., Jimenez, P. D., & Moorhead, A. R. (2015). The emergence of macrocyclic lactone resistance in the canine heartworm, Dirofilaria immitis. *Parasitology*, *142*(10), 1249–1259. https://doi.org/10.1017/S003118201500061X

Zhang, J., Xue, F., & Chang, Y. (2008). Structural Determinants for Antagonist Pharmacology That Distinguish the ρ1 GABAC Receptor from GABAA Receptors. *Molecular Pharmacology*, *74*(4), 941–951. https://doi.org/10.1124/mol.108.048710

APPENDICES

A1. qPCR primer information

Gene	Genbank accession number	Primer sequences Forward and Reverse (5' to 3')	Tm (°C)	%GC	Amplicon length (bp)
GLC-2	N/A	AGGAAACCTGGTGTTGGTAGTGAC	61.35	50.00	101
		CAAGCATAGGTTCCTGTATTAGTGTGA	61.52	40.74	
GLC-4	N/A	CAGAATGAACGGAATGGATGG	60.13	47.62	110
		GCCAATATCAATGTTAATCTGCG	59.59	39.13	
LGC-49	N/A	CAGTAAAATTGCTGAGATTCACGAA	60.94	36.00	93
		CGAACTCTATAATTGACCCAAACAG	59.70	40.00	
GAPDH	JQ780095.1	GGGAAACTGTGGCGAGATGG	62.47	60.0	138
		CGGAGTTGGCACACGAAAAG	61.43	55.0	
DITPH	JX469415.1	AAGGTCGACAAGTGGTGAGAA	56.99	47.62	169
		GTAGCCATATCTTCGTAACAGTTC	55.36	41.67	

A2. Standard curves for qPCR primers

Adult female - GAPDH

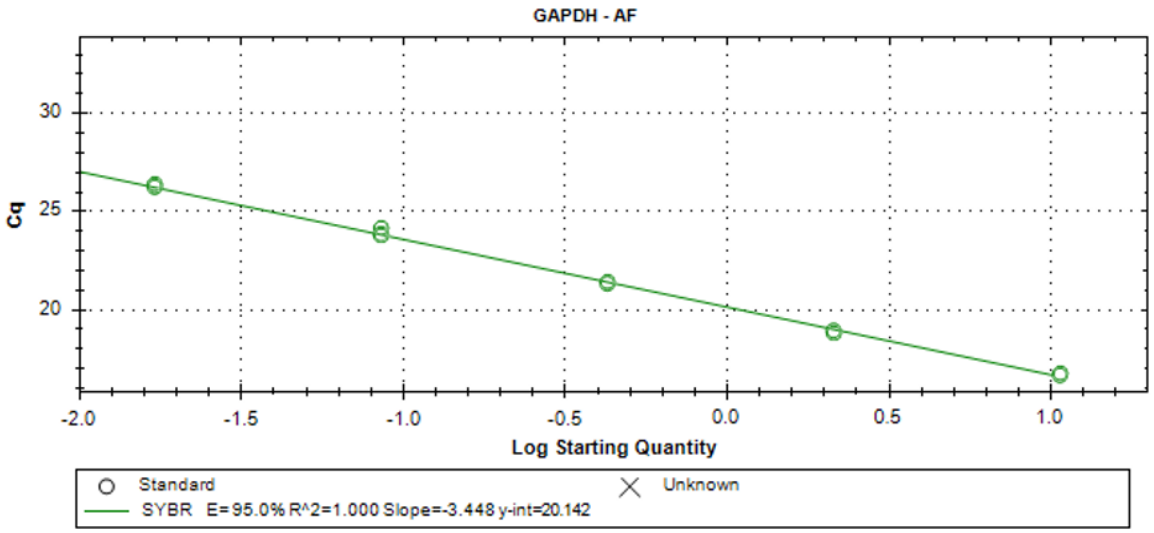

Adult female - DITPH

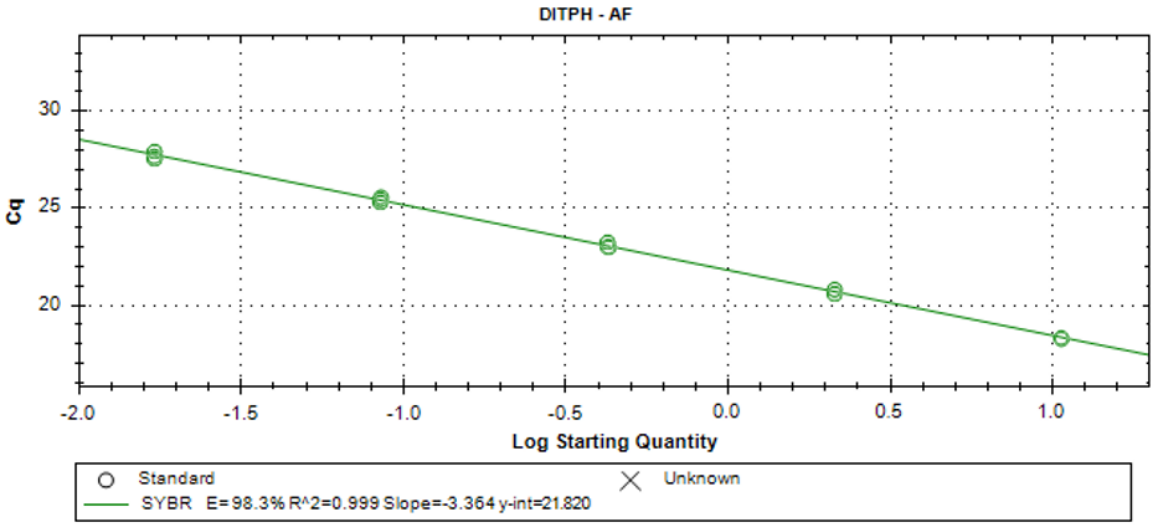

Adult female – GLC-4

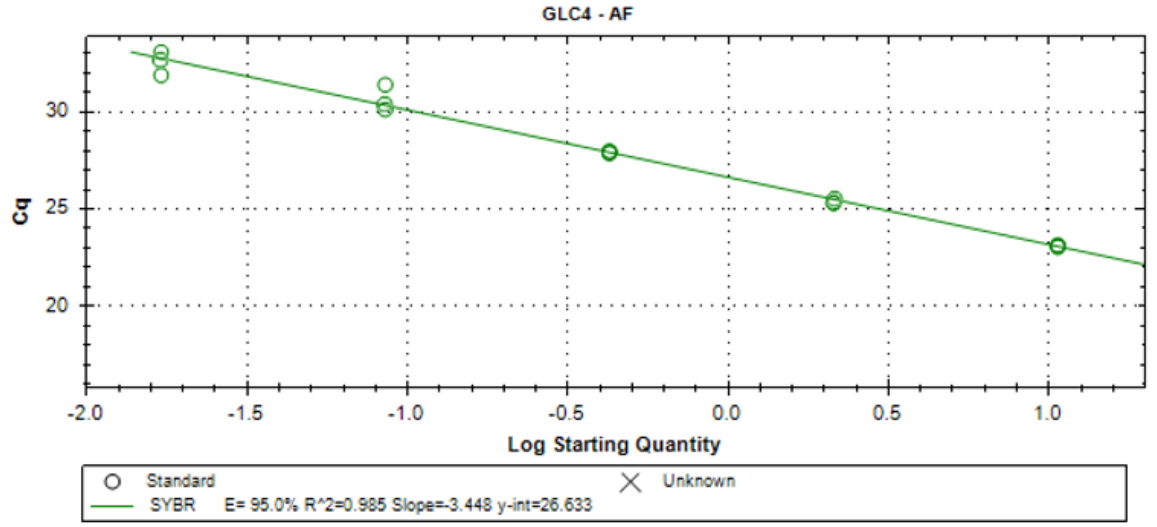

Adult female – GLC-2

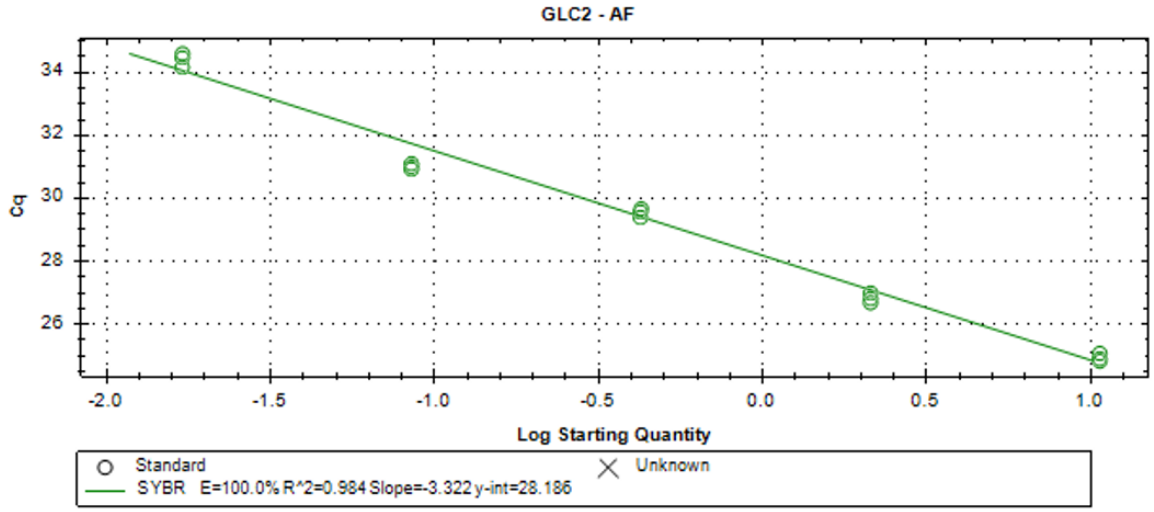

Adult female – LGC-49

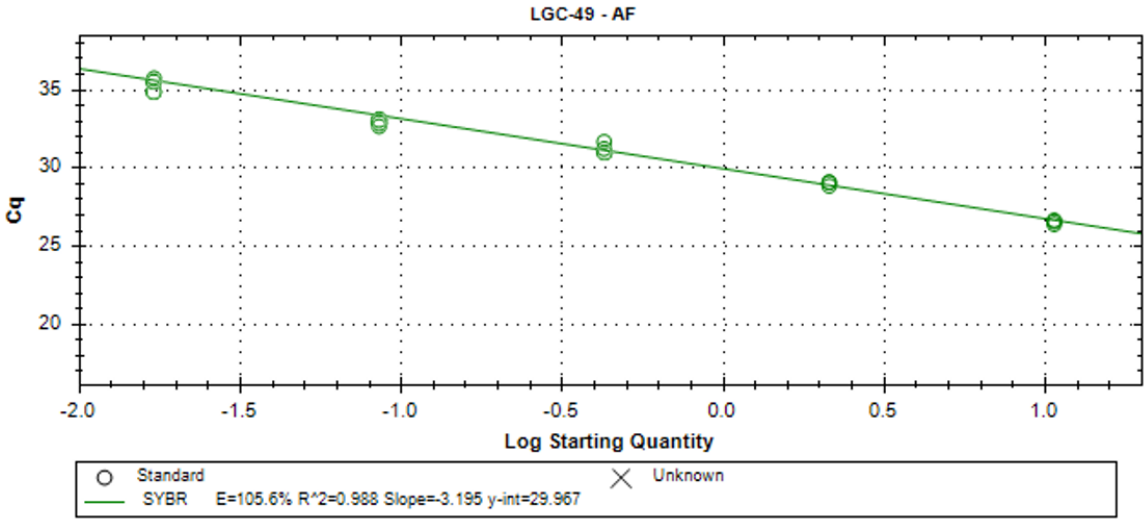

Adult male – GAPDH

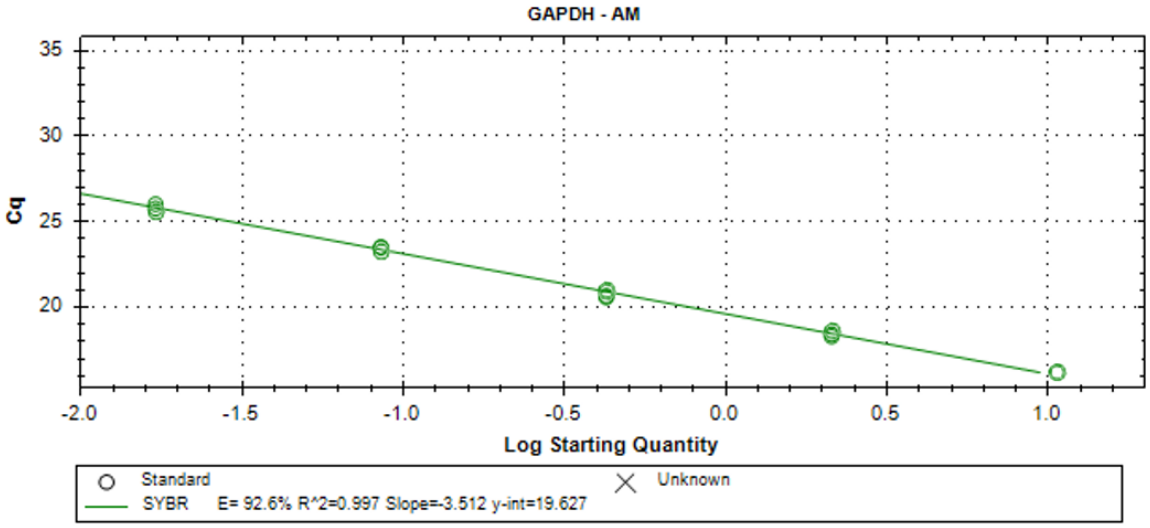

Adult male – DITPH

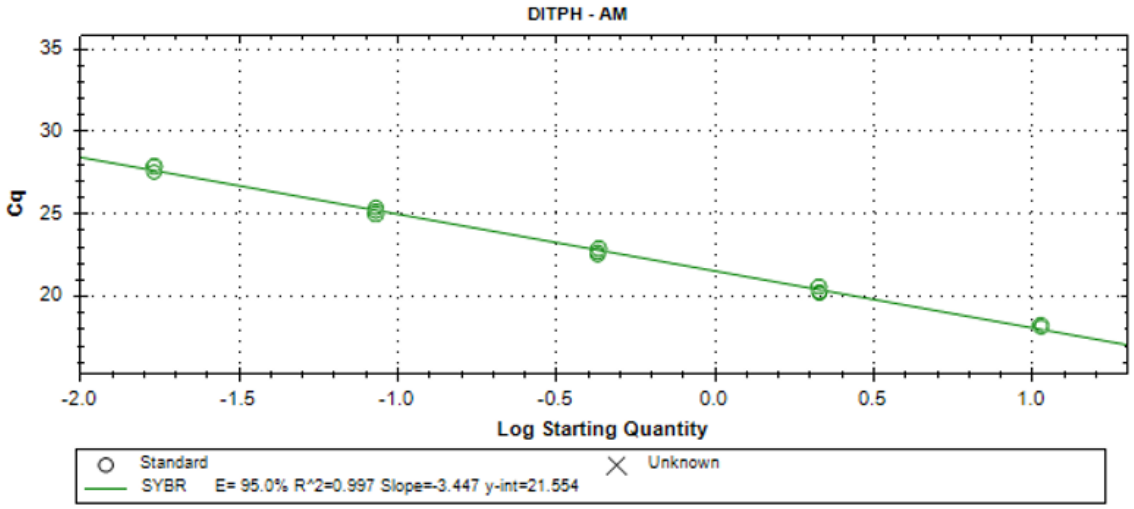

Adult male – GLC-4

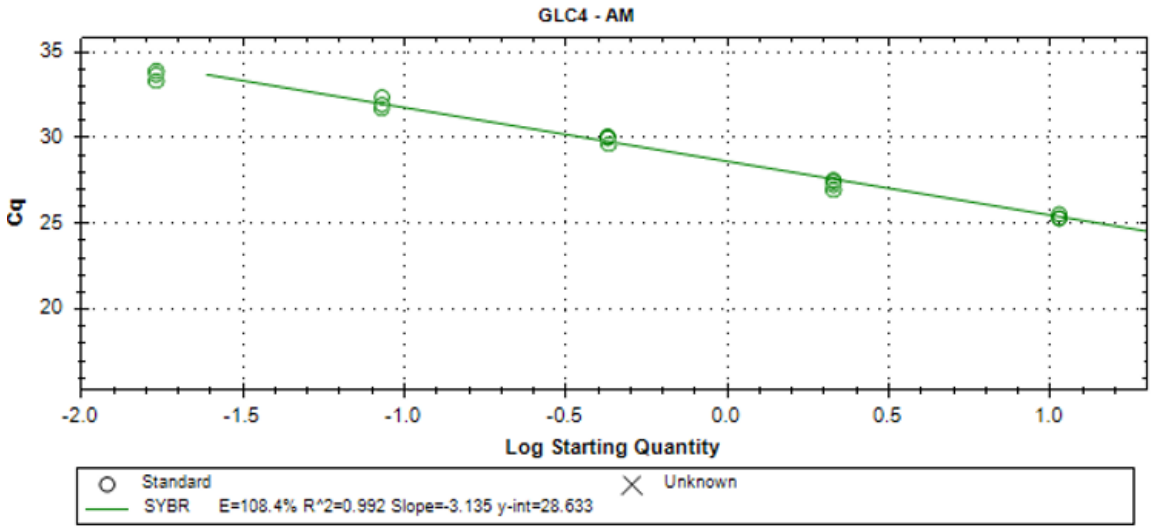

Adult male – GLC-2

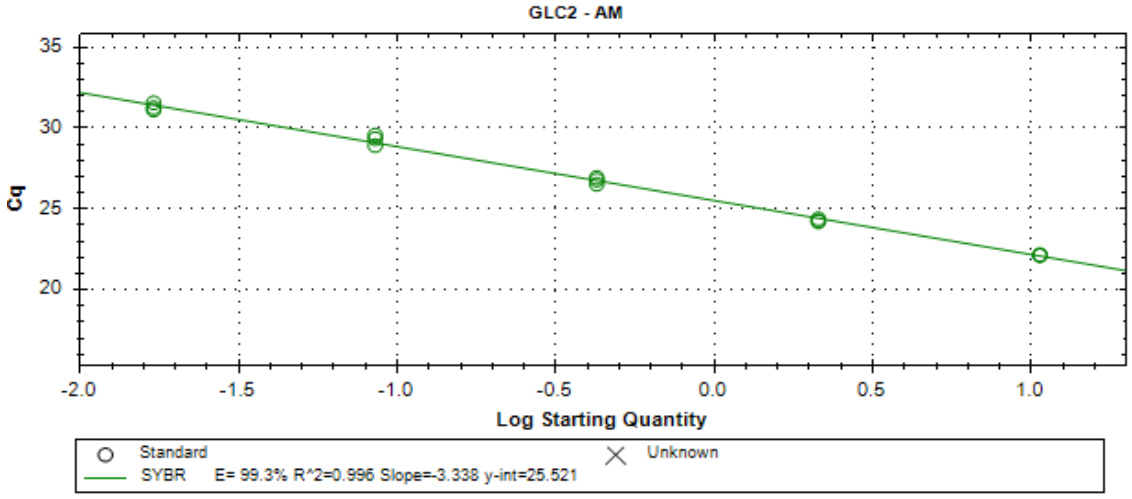

Adult male – LGC-49

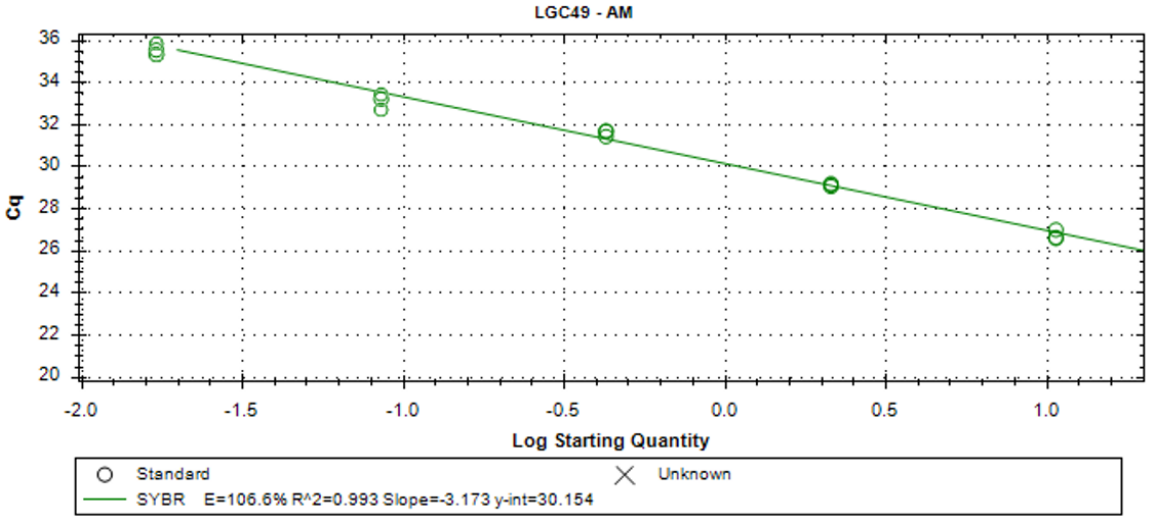

Microfilaria – GAPDH

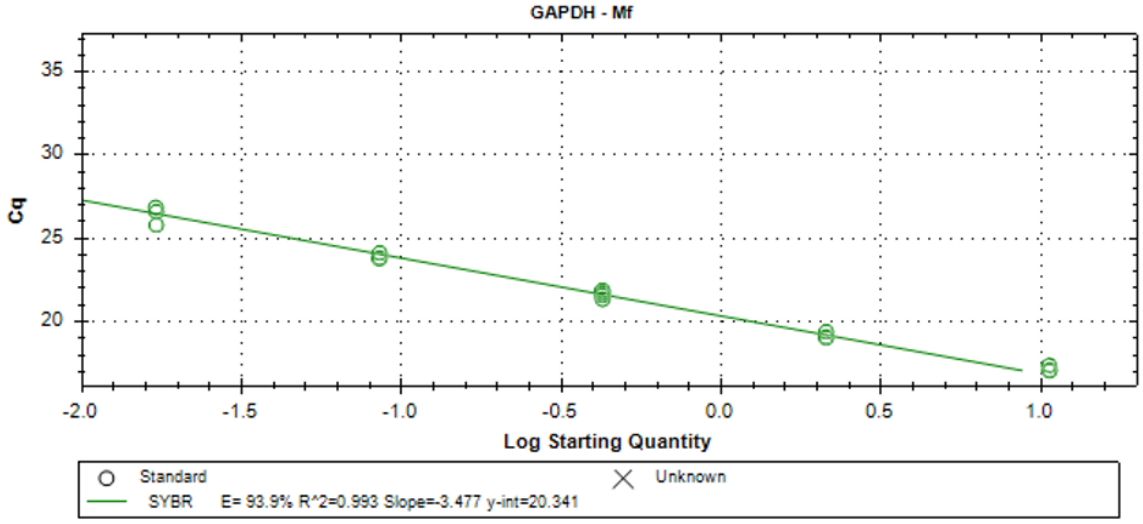

Microfilaria – DITPH

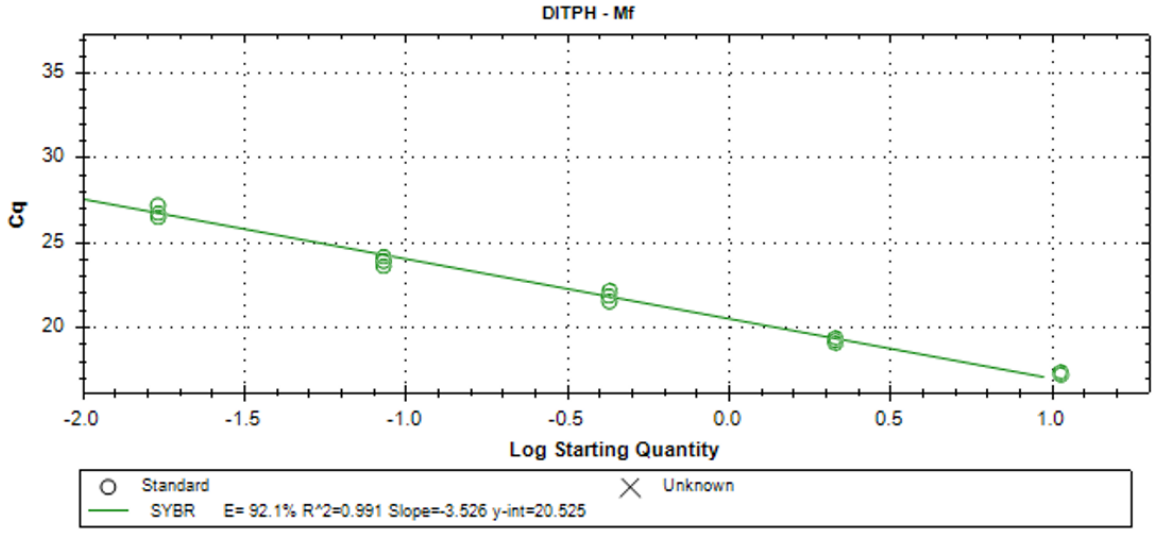

Microfilaria – GLC-4

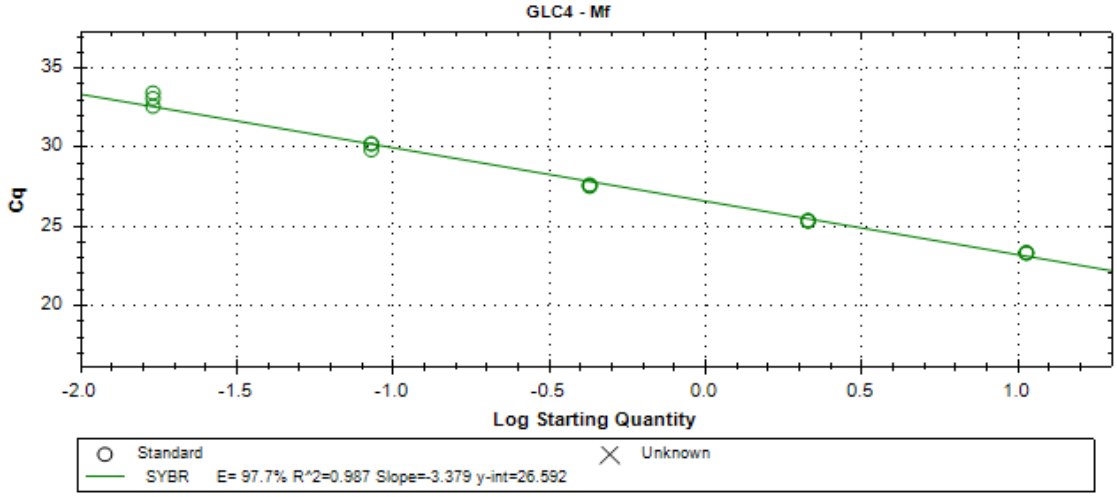

Microfilaria – GLC-2

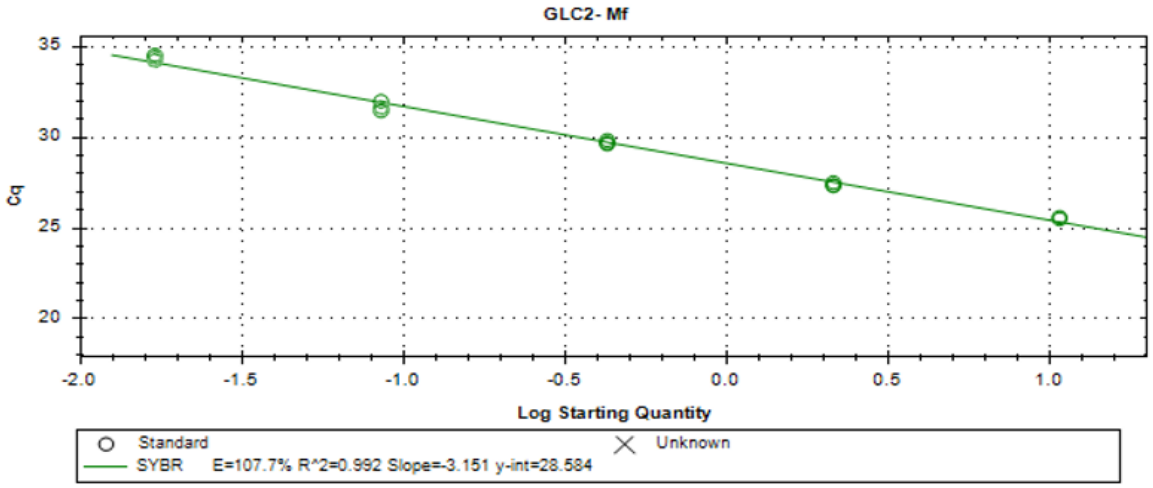

Microfilaria – LGC-49

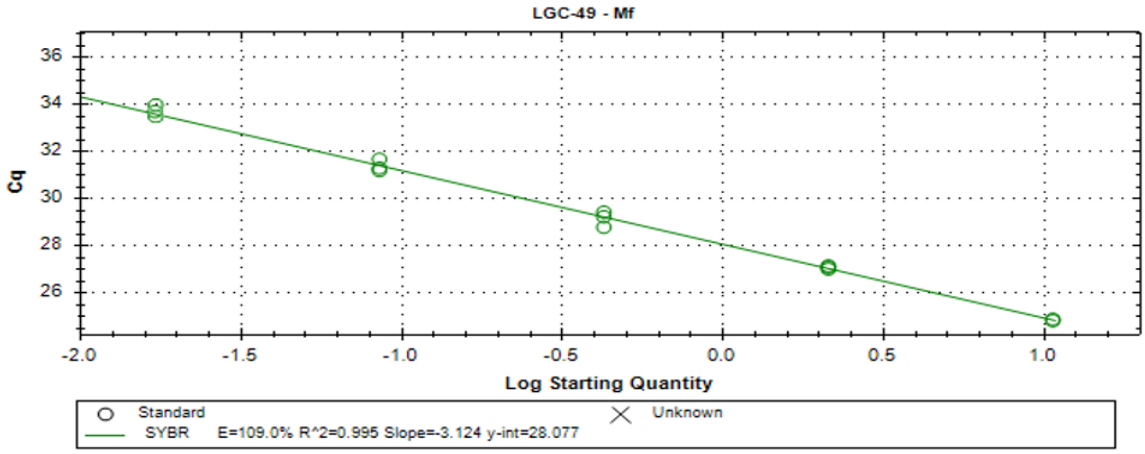

A3. qPCR primer linearity and efficiency values

Gene	Adult Male		Adult Female		Mf	
	E (%)	R^2	E (%)	R^2	E (%)	R^2
LGC-49	106.6	0.993	105.6	0.988	109.0	0.995
GLC-2	99.3	0.996	100.0	0.984	107.7	0.992
GLC-4	108.4	0.992	95.0	0.985	97.7	0.987
GAPDH	92.6	0.997	95.0	1.000	93.9	0.993
DITPH	95.0	0.997	98.3	0.999	92.1	0.991

*E = primer percent efficiency; R^2 = linearity correlation